Viscous Compressible Slip Flows. Part 2 : Meshless Solver for Rotating Slip Flows

Ajit Kumar Mahendra[*,1], G.Gouthaman[1] and R.K.Singh[2]
1Machine Dynamics Division, 2Reactor Safety Division,
Bhabha Atomic Research Centre,
Trombay, Mumbai, 400094, India.
*e-mail: mahendra@barc.gov.in

ABSTRACT
The Part 1 presented kinetic treatment of the slip flow and described kinetic flux vector splitting. The Part 2 of the paper presents the kinetic theory based approach for solving rotating slip flows. The paper describes numerical flow modeling of slip and rarefied flows. It also presents the meshless solver which makes use of least squares and Kinetic Flux Vector Splitting (KFVS) scheme and its Variance Reduction form (VRKFVS). The kinetic slip flow boundary condition is added with the Burnett terms which are quadratic in Knudsen number. The solver is able to capture slip flow features and typical features of the strongly rotating flows characterized by steep density gradient, supersonic flows, thin boundary layers towards the peripheral region with a rarefied central core.

Key words: meshless, least squares, kinetic, KFVS, VRKFVS, rotating, Chapman-Enskog distribution, Burnett, Boltzmann equation, rarefied, viscous, slip flow, second order slip

Nomenclature

$f(\vec{x}, \vec{v}, I, t)$	= molecular distribution function
f_0	= Maxwellian distribution function
f_1	= Chapman-Enskog distribution function
f_1^{Σ}	= total distribution at the wall undergoing diffuse and specular reflection
f_1^{in}, f_0^{wc}	= distribution incident to the wall and Maxwellian distribution at wall condition.
f_{RB}	= distribution associated with rigid body rotation
Δf, Δf_1	= difference in Maxwellian and their Chapman-Enskog term
$\Delta\hat{f}_1$	= difference between first order Chapman-Enskog and Maxwellian distribution
$\Delta\hat{f}_1$	= difference in 1st Chapman-Enskog expansion term for Maxwellian f_0 and f_M
$\vec{x}$, $\vec{v}$	= position vector and molecular velocity vector
I, I_0	= internal energy variable and average internal energy parameter
β	= thermal speed = $(2RT)^{-1}$
t_R	= relaxation time
t	= time
T, T_0	= temperature, average temperature
$\vec{u}$, $\vec{c}$	= macroscopic velocity vector, peculiar velocity
δu	= statistical fluctuation
N	= sample size used in DSMC
γ	= ratio of specific heat
p	= pressure
τ	= shear stress tensor
ρ	= density

R	= specific gas constant
E	= energy
$J(f, f)$	= binary collision term
Ψ, ψ_i	= moment and its element
λ	= mean free path
Kn, Kn_{GL}	= Knudsen number and gradient length Knudsen number
ς	= macroscopic parameter for gradient length Knudsen number calculation
V	= bulk velocity
V_Z, $V_{Z\max}$	= axial velocity and maximum axial velocity in the annuli
μ	= viscosity
M	= Mach number
$\vec{q}$	= heat flux vector
Pr	= Prandtl number
φ	= dissipation control function
ω	= angular velocity
r, r_{wall}	= radius and radius of the cylinder
z	= axial variable
θ	= azimuthal variable
U	= state update vector or vector of conserved variable = $[\rho, \rho\vec{u}, \rho E]^T$
U_M	= vector of conserved variable for Maxwellian f_M
GX, GY, GZ	= flux vector in x, y, z-direction
$GX_I^{\pm}$, $GY_I^{\pm}$, $GZ_I^{\pm}$	= inviscid flux vector in x, y, z-direction
$GX_v^{\pm}$, $GY_v^{\pm}$, $GZ_v^{\pm}$	= viscous flux vector in x, y, z-direction
GR	= radial flux component
S	= source terms
v_z	= axial velocity
v_r	= radial velocity
v_θ	= azimuthal velocity
ε	= Rossby number
Ω_z	= axial vorticity vector
σ	= diffuse reflection or accommodation coefficient
σ_v, σ_T	= momentum and thermal accommodation coefficient
u_s, u_w	= slip velocity and wall velocity
u_λ	= tangential gas velocity at one mean free path
n, s	=subscript denoting the normal and tangential coordinate to the wall
χ	= baroclinic term
r_i, r_0	= inner and outer radius
r_d	= dimensionless radius
d_h	= hydraulic diameter of the annuli
$\delta(BGK/HS)$	= first order slip parameter
A_1	= first order velocity slip coefficient associated with shear stress tensor
A_2	= second order velocity slip coefficient associated with shear stress tensor
C_1	= first order slip coefficient associated with heat flux vector for velocity slip
B_1	= first order slip coefficient for temperature jump
B_2	= second order slip coefficient for temperature jump
α_g	= viscosity coefficient
$\alpha(\sigma_v)$, $D(\sigma_v)$	= parameter as a function of tangential momentum coefficient in viscosity relationship

$\tilde{y}$	$= y/\lambda$
u_B, u_{NS}, u_{Kn}	= velocity based on Boltzmann, and Navier-Stokes solution its Knudsen contribution.
Δu_S	= Burnett addition to the slip velocity
rf	= relaxation factor
A, B	= parameters to calculate the analytical velocity profile
d(P_i,P_j)	= Euclidean distance between points P_i and P_j
sC	= sub-cloud of points
Bc	= sub-cloud of points lying in non-computing domain
h	= distance parameter
$N(P_o)$	= connectivity set for point P_o
ϕ_o, ϕ_i	= variable for determination of derivative at point P_o and P_i
x_o, y_o, z_o	= coordinates of the point P_o
x_i, y_i, z_i	= coordinates of the point P_i
Δx_i, Δy_i, Δz_i	= difference in coordinate distance for the points P_i and P_o
$\Delta\phi_i$	= difference in variable for the points P_i and P_o
ϕ_{xo}, ϕ_{yo}, ϕ_{zo},	= derivative of the variable with respect to x, y, z.
ex_i, ey_i, ez_i	= scaled error terms for the point P_i
$N_x^{\pm}(P_o)$	= split connectivity sub-stencil for x direction
$N_y^{\pm}(P_o)$	= split connectivity sub-stencil for y direction
$N_z^{\pm}(P_o)$	= split connectivity sub-stencil for z direction
nx,ny,nz	= number of points in the connectivity sub-stencil for x,y,z direction
Φ_o	= matrix of derivatives ($[\phi_{xo}, \phi_{yo}, \phi_{zo}]^T \in \mathrm{R}^n$)
$\Delta\phi_N$	= matrix of observation ($[\Delta\phi_1, \Delta\phi_2, \ldots, \Delta\phi_m])^T \in \mathrm{R}^m$)
A_N	= least square data matrix used in normal equations approach ($\in \mathrm{R}^{n\times m}$)
η_i	= slope of the connectivity point P_i
C	= least square matrix
$\lambda_e^{\pm}$	= eigen values of the least square matrix C

1. INTRODUCTION

The Part 1 of the paper gives an overview of kinetic theory and its application to fluid flow and describes BGK model, construction of Chapman-Enskog distribution and kinetic flux vector splitting scheme (KFVS). KFVS for viscous flows applies Courant splitting at the Boltzmann level followed by moment-method strategy using Chapman-Enskog distribution to obtain split Navier-Stokes equations. The Part 1 of the paper also describes variance reduction kinetic flux vector splitting (VRKFVS), diffuse reflection model based slip boundary treatment.

Part 2 describes the numerical modelling of rarefied, rotating slip flows. For rapidly rotating viscous compressible flows confined between two concentric rotating cylinders the gas undergoes rigid-body rotation. The rigid-body rotation is characterized by an exponential density rise in the radial direction towards the periphery with thin boundary layers and a rarefied inner core [1,2]. Majority of the researchers Dickson and Jones[3], Park and Hyun [4] and Babarsky *et al*. [5] focused more on perturbative flows arising out of basic state of rigid body rotation using continuum hydrodynamics even though a large portion of the volume in the central core is rendered rarefied near to the free molecular region. The flow predicted by kinetic theory differs from the results obtained using continuum hydrodynamics [6]. Based on the Boltzmann equation Müller [7] concluded that in rotating systems a radial temperature gradient apart from leading to the radial heat flux also causes tangential heat flux which are related at the level of the Burnett approximation. Research of Sharipov and Kremer[8,9] and Sharipov et. al.[10] have further confirmed that the transport equations in non-inertial frames creates an anisotropy and brings qualitatively changes in the transport properties of the fluid making it different from those in inertial frame of rotation. Investigations [8-10] to study the transport phenomena through a fluid confined between two coaxial cylinders over a wide range of gas rarefaction revealed that the kinetic approach do not follow from the Navier-Stokes equations of continuum mechanics. Taheri and

Struchtrup [11] have used continuum approach as well as regularized 13-moment (R13) equations to study the effects of rarefaction in micro flows between two rotating coaxial cylinders. Numerical modeling of high speed rotating flows is a challenge as the regime changes from continuum at the periphery, slip, transition to non-continuum in the central core. Such a flow is of considerable interest and importance in the field of hydrodynamic bearings, rotating machinery and heat exchangers.

The most common approach to simulate such a flow is to couple the continuum solver with the slip boundary condition. The slip boundary condition should effectively capture slip flow features under combined effects of adverse pressure gradient and rarefaction. Investigation reveals that there are large number of second order slip models existing in the literature each with its own geometric specific slip coefficient and range of validity in the non-continuum slip and transition region. Most of the slip models in the literature are for simple micro-channel flows. Slip velocity not only depends on the velocity gradient in the normal direction but also on the fluid dynamic gradients in the tangential flow direction. In such a scenario we require a more fundamental approach. The prime motivation of the paper is to simulate slip modeling through kinetic theory route. Treatment of slip boundary using kinetic upwind fluxes based on diffuse reflection model considers these variations in the tangential flow direction. The paper presents the kinetic upwind method for compressible rotating viscous slip flows by using meshless solver. In order to extend the simulation to non-continuum transition region an attempt has been made by adding the second order Kn^2 terms associated with the Burnett constitutive relations to the first order kinetic implementation of the slip. The paper describes the modified Split-stencil Least square Kinetic upwind method for Navier-Stokes (m-SLKNS) solver which belongs to Least square Kinetic Upwind Method (LSKUM) family[12-17] as it makes use of least squares and Kinetic Flux Vector Splitting (KFVS) scheme with kinetic slip flow boundary condition. KFVS for viscous flows applies Courant splitting at the Boltzmann level followed by moment-method strategy using Chapman-Enskog distribution to obtain split Navier-Stokes equations[17,18]. In this paper we have carried out numerical simulation of compressible rotating flows using modified kinetic flux vector scheme (m-KFVS) similar to Anil et. al. [19] by incorporating the modified Courant splitting based on Rossby number of the rotating flow. For strongly rotating flows a novel scheme Variance Reduction Kinetic Flux Vector Splitting (VRKFVS) is used so as to capture the weak secondary flow feature embedded in a strongly rotating flow field.

Most of the industrial problems have many components and generation of suitable grid around them becomes the bottleneck. Conventional approach requires grids which include structured multi-block meshes, chimera or overset grids, unstructured grids, Cartesian grids and hybrid grids. Recently meshfree or meshless methods have gained popularity. All meshless numerical methods share a common feature that no mesh is needed and the solver is capable of operating on an arbitrary distribution of points. The paper uses meshless method which is a modified form of Split-stencil Least square Kinetic upwind method for Navier-Stokes (m-SLKNS) similar to SLKNS solver. SLKNS [18] differs from Least square kinetic upwind method for Navier-Stokes (LSKUM-NS) [17] which uses normal equations approach to solve least square problem. SLKNS [18] avoids ill-conditioning encountered while using highly stretched distribution of points in the boundary layers. Further, m-SLKNS is able to handle steep density gradient and thin boundary layers towards the peripheral region as well as non-continuum features of rarefied regions using VRKFVS scheme.

2. NUMERICAL FLUID MODELLING FOR SLIP FLOWS

The presence of rarefied domain around space vehicle or fluid transport in microelectromechanical devices (MEMS) is a typical example of non-continuum flow feature[1]. One of the main difficulties in modeling such a flow is due to breakdown of continuum flow assumption as the mean free path of gas molecule is comparable or larger than characteristic dimensions of the flow system. Numerical fluid modelling depends on fluid regime defined by the extent of non-equilibrium effects and rarefaction. Breakdown of the continuum [20-23] and its fluid regime [24,25] is discussed in Part 1. The fluid modelling can be classified based on three approaches: (i) molecular modeling approach and (ii) continuum modeling approach, and (iii) hybrid approach. In the molecular modeling approach [26,27] the fluid is assumed to be collection of molecules which are to be solved either by deterministic or statistical methods. One of the main drawback of this probabilistic method is the occurrence of

[1] The main differences between conventional rarefied flow and fluid transport in MEMS are the operating pressure and extremely low Reynolds number (creeping flow) encountered in the latter.

statistical noise and inefficient handling near continuum flows and flows with recirculation. On the other hand the deterministic methods [28] based on solving the kinetic equation, namely the Boltzmann equation are very computationally expensive due to quadratic cost of the velocity discretization of the collision operator. In the continuum modelling approach the fluid is assumed to be continuous and indivisible. The macroscopic variables like velocity, density, pressure, etc. are defined at every point in space and time, and conservation of mass, energy and momentum lead to a set of nonlinear partial differential equations like Euler, Navier–Stokes, Burnett, etc. In the hybrid approach the non-continuum regions are solved using the molecular based methods and interfaced with the continuum regions [20,29]. The determination of non-equilibrium and continuum regions is generally carried out using a local continuum breakdown parameter called the gradient-length Knudsen number defined as

$$Kn_{GL,\varsigma} = \frac{\lambda}{\varsigma}|\nabla\varsigma| \cdot \tag{1}$$

where ς is the macroscopic parameter of interest and λ is the mean free path given as

$$\lambda = \mu\sqrt{\frac{\pi}{2\rho p}} \tag{2}$$

Table 1. gives the different fluid models and its regime.

Table 1. Knudsen number based fluid regime and fluid models.

Knudsen Number and flow regime	Fluid Model
Kn→0 Continuum convective flow	Euler Equations
Kn≤0.01 Continuum convective and diffusive flow	Navier-Stokes equations with no slip boundary condition
0.01≤Kn≤0.1 Continuum slip flow	Navier-Stokes with slip boundary condition Burnett equation with slip boundary condition DSMC, IP, Hybrid solvers
0.1≤Kn≤10 Transition flow	Burnett equation with slip boundary condition DSMC, IP, moment method, Lattice Boltzmann, Hybrid solvers
Kn>10 Free-molecular flow flow	Collisionless Boltzmann, DSMC, Molecular dynamics

2.1 Molecular based numerical schemes for slip flows

Molecular based numerical schemes such as direct simulation Monte Carlo (DSMC) becomes a useful tool for rarefied non-continuum flows. In DSMC method microscopic properties are averaged over a small space region to obtain the macroscopic state variables. For low speed rarefied flow the statistical scatter requires a huge sample size. For example consider the macroscopic velocity to be of the order 0.1 m/s with background noise under room condition given by $\sqrt{2RT}$ which is of the order 10^3 m/s. If we require signal to be nine times larger than the noise then the sample size N required is around 10^9 to keep the standard deviation given as $\sqrt{2RT/N}$ to a small enough value [30]. The signal-to-noise ratio for a dilute gas can be given as

$$\frac{u}{\delta u} = M\sqrt{\gamma N} \tag{3}$$

where u is the characteristic flow velocity, δu is the statistical fluctuation, M is the Mach number, γ is the ratio of specific heat and N is the sample size (refer Shen [27] for details). Thus, DSMC becomes costly to simulate rarefied low speed gas flows encountered in MEMS and micro-channel flows. DSMC finds more applications to many high speed flows. Fan and Shen [31,32] proposed information preservation (IP) method to tackle this problem of large sample size. The thermal movement of the particles causes statistical scatter in DSMC while in IP method it surfaces only at the macroscopic information level. In IP each simulated particle is assigned two velocities : thermal velocity c and information velocity (IP velocity) u. Thus, each simulated particle carries sum of the macroscopic velocity of a gas flow as well as velocity scatter with an aim to preserve and update the macroscopic information thereby reducing the statistical scatter. The major advantage of IP method is the considerable reduction in the sample size. For the same example given earlier for the low speed flows the sample size required for IP method is around 10^3 to 10^4. Another advantage of the IP method is the implementation of the boundary condition as macroscopic values of the flow field are known at each time step. Since IP method handles more information than the DSMC method hence it more memory intensive and complicated in its implementation. Another drawback of IP method is the issue of stability as the time step cannot be large and particle sample size cannot be small.

2.2 Direct numerical solution (DNS) of Boltzmann equation

The modelling of the collision term poses a challenge because of its non-linear nature. The numerical methods should satisfy all the properties desired for a kinetic models described in Part 1 of the paper i.e. properties of locality and Galilean invariance, additive invariants, local entropy production, etc. There are broadly three methods for direct solution of the Boltzmann equation[28] i) node to node (NtN) method, ii) Tcheremissine's method, and iii) node to closest node (NtCN) method. In the NtN method [33-35] a collision sphere in velocity space is wrapped around pre- and post collision velocities. The NtN method takes into account only those post-collisional velocities that fall exactly into the nodes of the velocity grid. Tcheremissine's method [36] is a generalization of the NtN method for more complex models of the collisions by taking into account inverse collisions that do not fall into the nodes of the velocity grid. NtCn method [37] on the other hand can be used for arbitrary interaction potentials and non-uniform grid in velocity space.

2.3 Hybrid solvers

DSMC becomes an expensive numerical method due to high sample size to keep the stochastic noise bounded to a lower value. DSMC also becomes impractical for time dependent flows as ensemble averaging becomes prohibitively expensive. Near the continuum regions it becomes impractical to apply DSMC as mean free time is very low. On the other hand continuum solvers like Navier-Stokes are not valid in the rarefied as well as in the non-thermodynamic regions of shock. Many researchers [20,22,29] have used a hybrid approach to accommodate both the issues of accuracy and computational cost for problems that contain the disconnected rarefied and non-equilibrium kinetic regions in the continuum flow domain. DSMC due to its inherent statistical noise has been identified as an obstacle for the development of hybrid solvers [38]. Some group of researchers [20] has developed hybrid solvers which employs deterministic kinetic Boltzmann solver instead of DSMC for rarefied and continuum gas flows. Typical hybrid solver dynamically adapts the meshes with addition and deletion of kinetic patches to simulate the rarefied and non-continuum regions embedded in the continuum flow domain.

The most crucial aspect of the hybrid codes are the : i)adequate continuum breakdown parameter, ii)identification of non-continuum regions, iii)method of domain decomposition , and iv) coupling strategy i.e. imposition of boundary conditions at the interface and procedure for information exchange. For example there are three methods of domain decomposition. The first method is domain decomposition in physical space using appropriate continuum breakdown criteria. The second method is domain decomposition in velocity space where fast and slow particles are treated separately [39]. The third method is the hybrid of the two in which one solves kinetic and fluid equation in entire domain. For example, Beylich [40] interlaces the path-integral form of the kinetic equation (Boltzmann level) with the set of conservation equations (Navier-Stokes level). The coupling strategy between continuum and non-continuum domain can either be flux based coupling or state based coupling [29,41]. In the flux based coupling fluxes of mass, momentum and energy are calculated according to non-continuum and continuum domains. In this method the fluxes at the interface are modified such that fluxes of continuum and non-continuum equate and conservation is insured in the transfer of information across the interface. State based coupling is inherently conservative; in this approach macroscopic state is obtained by using the average particle information in the non-continuum region and distribution of particles are generated from a macroscopic state on the other side of the interface in the continuum region.

The major drawback of hybrid solvers is poor computational efficiency and the ability to simulate unsteady flows. Identification of non-continuum regions and implementation as well as synchronization of two separate methods for continuum and rarefied flow simulation makes the hybrid solver quite complex.

2.4 Treatment of slip flow based on higher order continuum equations

Most common kinetic theory based approach is either based on i) 5 moments based on expansion of distribution function (Chapman-Enskog series solution leading to Burnett or super-Burnett equations) or ii) higher moment based approach which include Grad's 13 moment approach, Struchtrup's regularized R13, etc. Lockerby *et. al* [42] have investigated most of the common higher order continuum equations and kinetic theory based approach. The study revealed that most of these approaches fail to capture Knudsen layer structure in Kramers' problem shown in figure 1. Kramers' problem considers unidirectional isothermal motion of a gas over a stationary planar solid. In the Kramers' problem as the normal distance from the surface, $y \rightarrow \infty$ the bulk flow gradient du/dy becomes constant, where u is the tangential flow velocity. Let $u_B = u_{NS} + u_{Kn}(y)$ be the true flow-field based on the Boltzmann solution where u_{NS} the Navier-Stokes based slip flow approximation and $u_{Kn}(y)$ is the Knudsen layer correction [56, 57]. Similarly for temperature we can write $T_B = T_{NS} + T_{Kn}(y)$ where T_{NS} the Navier-Stokes based temperature field approximation and $T_{Kn}(y)$ is the Knudsen layer correction. The Knudsen layer correction $u_{Kn}(y)$ and $T_{Kn}(y)$ decay quickly as $y/\lambda \rightarrow \infty$. Hadjiconstantinou [56] estimates $u_{Kn}(y)$ decays to approximately 3% of its maximum value at $y = 1.5\lambda$ referred as effective width of the Knudsen layer. The Navier-Stokes solution reveals that the terms of order Kn^2 needs to be superimposed to the Navier-Stokes solution to capture the true solution of the Boltzmann equation for the Kramers' problem. Lockerby *et. al* [42] investigations have revealed that for low-speed isothermal flows neither Burnett [41], super-Burnett[44], or Grad's 13[45] moment equations can model the Knudsen layer. However, some of the higher order accurate continuum equations can qualitatively model the Knudsen layer. Modeling of Knudsen layer can be achieved either by introducing corrections based on kinetic theory or by wall function approach based on suitable scaling of stress-strain relationship. Table 2. gives the list of higher continuum models and their capabilities to capture Knudsen layer structure in Kramers' problem compiled from Lockerby *et. al* [42].

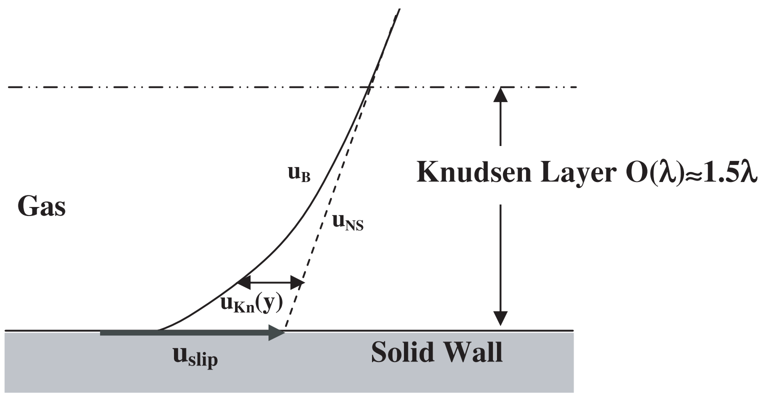

Figure 1. Knudsen layer in the Kramers' problem

Table 2 Higher continuum models and their capability to capture Knudsen layer structure.

Higher Continuum models which fail to predict Knudsen layer structure	Higher Continuum models which predict Knudsen layer structure
Burnett (Chapman and Cowling [43])	Linearized Boltzmann (Cercignani [30,50,75])
Super-Burnett (Wang Chang[44])	BGK model (Loyalka and Hickey[65])
Grad's 13 (Grad [45])	Zhong's augmented Burnett (Zhong[52])
Wood's (Wood [46])	Regularized Burnett (Jin and Slemrod[53])
Lumpkin's reduced Burnett (LumpkinIII [47])	R13 (Struchtrup & Torrilhon[54])
Eu's GH (Eu [48])	BGK Burnett (Balakrishnan[55])

2.5 Treatment of slip flow based on slip models and Navier-Stokes equation

Harley *et al*. [58], Arkilic *et al* [59], Beskok and Karniadakis [60] have shown that Navier-Stokes equations coupled with first order velocity slip and temperature jump boundary conditions effectively captures slip flow. One of the earliest model is the Maxwell's velocity slip [61] expressed in conventional form as

$$u_s - u_w = \pm\left(\frac{2-\sigma_v}{\sigma_v}\right)\lambda\left(\frac{\partial u_s}{\partial n}\right)_w + \frac{3}{4}\frac{\mu}{\rho T}\left(\frac{\partial T}{\partial s}\right)_w \cdot \tag{4}$$

This can be expressed in general form [62] as

$$u_s - u_w = \pm\left(\frac{2-\sigma_v}{\sigma_v}\right)\frac{\lambda\tau_{sn}}{\mu} - \frac{3}{4}\frac{\Pr(\gamma-1)}{\gamma\, p}q_s \tag{5}$$

where subscript n denotes the normal coordinate to the wall, s is the tangential coordinate, τ_{sn} is the component of shear stress, q_s is the component of heat flux vector, γ is the ratio of the specific heats, u_s is the slip velocity, u_w is the reference wall velocity and Pr is the Prandtl number. The second term on the right hand side of the equation is the thermal creep contribution to the slip velocity due to tangential temperature variation. Similarly, von Smoluchowski's temperature-jump boundary condition [63] is

$$T_s - T_w = \left(\frac{2-\sigma_T}{\sigma_T}\right)\frac{2\gamma}{\Pr(\gamma+1)}\lambda\frac{\partial T}{\partial n} \tag{6}$$

where σ_v and σ_T are the tangential momentum and thermal accommodation coefficients respectively. The accommodation coefficients depend upon specific gas and the surface quality and it models the momentum and energy exchange of gas molecules impinging on the walls. These relations, to first order in Knudsen number for velocity slip and temperature jump can also be expressed as

$$u_s - u_w = \pm A_1\frac{\lambda\tau_{sn}}{\mu} - C_1\frac{\Pr(\gamma-1)}{\gamma\, p}q_s \tag{7}$$

$$T_s - T_w = B_1\frac{2\gamma}{\Pr(\gamma+1)}\lambda\frac{\partial T}{\partial n} \tag{8}$$

where coefficients $A_1 = \left(\frac{2-\sigma_v}{\sigma_v}\right)$, $C_1 = \frac{3}{4}$ are given by Maxwell and $B_1 = \left(\frac{2-\sigma_T}{\sigma_T}\right)$ is given by von Smoluchowski. These coefficients can also be estimated by solving the Boltzmann equation for slip coefficients for BGK model and HS model i.e $\delta(BGK/HS, \sigma_v = 1)\left(\frac{2}{\sqrt{\pi}}\right)$. Rigorous kinetic approach of Albertoni *et al*. [64], Loyalka et. al. [51], Loyalka and Hickey [65], Loyalka and Tompson [66] have shown that $\delta(\sigma_v = 1)$ is 1.016191 for BGK molecules. The first order slip coefficient A_1 using kinetic approach for BGK molecular model can be written as

$$A_1 = \delta(BGK, \sigma_v = 1)\left(\frac{2}{\sqrt{\pi}}\right) = 1.14665 \cdot \tag{9}$$

Ohwada et. al.[67] evaluates $\delta(\sigma_v = 1)$ as 0.98738 for HS molecules. The first order slip coefficient using kinetic approach for HS molecular model can be written as

$$A_1 = \delta(HS, \sigma_v = 1)\left(\frac{2}{\sqrt{\pi}}\right) = 1.114139 \cdot \tag{10}$$

The other coefficients C_1 and B_1 for fully accommodating surfaces $\sigma = \sigma_v = 1$ for BGK model are $C_1(BGK, \sigma = 1) = 1.149$ and $B_1(BGK, \sigma = 1) \approx 1.168$. For hard sphere (HS) model Ohwada et. al.[67] evaluates these coefficients as $C_1(HS, \sigma = 1) = 1.015$ and $B_1(HS, \sigma = 1) = 1.13$. For isothermal flows of real gases the hard sphere model is more appropriate compared to BGK.

As described earlier the Knudsen layer correction $u_{Kn}(y)$ over Navier-Stokes solution u_{NS} requires terms of order Kn^2 provided by second order velocity slip model. Experimental studies [70,71,77] have also shown that first order slip model do not compare well with the experimental data beyond *Kn>0.1*. Most of the research is based on simple micro channel flow or flows in simple geometry without any flow separation. Thus, behavior of the slip model in the recirculation zone due to combined effect of rarefaction and reduction of Reynolds number forms a good validation test [72,73]. Modeling the non-equilibrium layer close to the walls, known as the Knudsen layer is the most crucial aspect for obtaining a reliable higher-order slip model. Physics based empirical slip model of Beskok [72] predicts Knudsen's minimum, observed around $Kn \approx 1$ as well as the flow rate, velocity profile, and the pressure distribution. Beskok [72] carried out detailed study of the slip model and validated it with DSMC results for classical backward facing step under combined effect of rarefaction and adverse pressure gradient on separated flows as a function of the Reynolds and Knudsen numbers. Beskok [72] slip equation is based on tangential gas velocity one mean free path away from the wall surface as follows :

$$u_s = \frac{1}{2}\left[u_\lambda + (1-\sigma_v)u_\lambda + \sigma_v u_w\right] \tag{11}$$

where u_λ is the tangential gas velocity one mean free path away from the wall surface and u_s is the slip velocity. Using the Taylor series expansion of u_λ about u_s results in the following equation :

$$u_s = \frac{1}{2}(2-\sigma_v)\left[u_s + \lambda\left(\frac{\partial u}{\partial n}\right)_s + \frac{\lambda^2}{2}\left(\frac{\partial u}{\partial n}\right)_s + \ldots\right] + \frac{1}{2}\sigma_v u_w \cdot \tag{12}$$

Another example of higher order slip is linearized Maxwell-Burnett boundary condition obtained by Lockerby *et al*. [62] using the Burnett constitutive relations, the expressions of slip are as follows

$$\begin{aligned} u_s - u_w \quad &= \pm\left(\frac{2-\sigma_v}{\sigma_v}\right)\lambda\left(\frac{\partial u_s}{\partial n} + \frac{\partial u_n}{\partial s}\right)_w + \frac{3\mu}{4\rho T}\frac{\partial T}{\partial s} \pm \left(\frac{2-\sigma_v}{\sigma_v}\right)\lambda\left(2\frac{\mu}{\rho^2}\frac{\partial^2 \rho}{\partial s \partial n} - \frac{\mu}{\rho T}\frac{\partial^2 T}{\partial s \partial n}\right)_w \\ &+ \frac{3\Pr}{16\pi}\left(\frac{\gamma-1}{\gamma}\right)\lambda^2\left((45\gamma-61)\frac{\partial^2 u_s}{\partial s^2} + (45\gamma-49)\frac{\partial^2 u_n}{\partial s \partial n} - 12\frac{\partial^2 u_s}{\partial n^2}\right)_w \cdot \end{aligned} \tag{13}$$

For stationary flow based on the linearized Maxwell-Burnett boundary condition, the thermal stress flow due to temperature gradients can be derived as.

$$u_s - u_w \quad = \pm\left(\frac{2-\sigma_v}{\sigma_v}\right)\lambda\left(-\frac{\mu}{\rho T}\frac{\partial^2 T}{\partial s \partial n}\right) \cdot \tag{14}$$

Higher order slip condition in Knudsen number approaches the classical Maxwell's first order condition if we neglect second and higher order terms. A second or higher order slip boundary condition requires corresponding higher order continuum model i.e. second order slip condition will require Burnett equation. Struchtrup and Torrilhon [74] have used R13 equations for the expression of the higher order slip boundary. Many researchers have used the generalized second-order velocity slip boundary condition, which in absence of thermal creep contribution can be expressed as

$$u_s - u_w = \pm A_1 \lambda \left(\frac{\partial u_s}{\partial n} \right)_w - A_2 \lambda^2 \left(\frac{\partial^2 u_s}{\partial n^2} \right)_w \tag{15}$$

where A_1 and A_2 are the first and second order slip coefficients. For flow problems with small Knudsen number the solution of linearized Boltzmann equation using asymptotic approaches can be used to obtain the second slip coefficient. For example Cercignani and Lorenzani [75] have obtained the solution of Navier-Stokes solution by using the second order slip boundary condition for Poiseuille mass flux problem as

$$S_{NS} = 1 + 6A_1 Kn + 12A_2 Kn^2 \cdot \tag{16}$$

Cercignani and Lorenzani [75] have used the variational technique to solve Boltzmann equation to get asymptotic near-continuum solution for the Poiseuille mass flux to obtain the slip coefficients. The Navier-Stokes solution reveals that the second order coefficient A_2 with the terms of order Kn^2 needs to be superimposed to the Navier-Stokes solution to capture the true solution of the Boltzmann equation. Thus, the Knudsen layer correction $u_{Kn}(y)$ over Navier-Stokes solution u_{NS} requires a second order velocity slip model. With the second order slip coefficient the classical hydrodynamical equations can simulate beyond $Kn = 0.1$ i.e. second order model extends its applicability beyond slip flow regime into the transition regime. Since the cost of solution of Navier-Stokes is negligible compared to the alternative methods hence large number of of researchers have attempted to develop second order slip models that can be used beyond $Kn = 0.1$.Table 3 gives the value of different slip coefficients proposed in the literature for gas micro flows.

It can be inferred from the table that the first order slip coefficient is mildly dependent on molecular interaction model as compared to strong dependence seen in second order slip coefficient. Most of the theoretically derived second order slip models are derived under linearized conditions for flat walls, steady flow and small gradients. The real conditions can be quite different as geometries can be complex, flow can be time dependent, etc. The table reveals that there is a large discrepancy between the values of the second order coefficient and there seems to be no consensus amongst the researchers even for the simple flows. It is also most likely that second order coefficient A_2 is geometry dependent. Under such a scenario boundary condition based on set of Burnett equations [62] looks most promising as it includes the terms of order Kn^2, shows reasonable agreement with experimental data and is simple to implement numerically.

Since the first order slip coefficient itself depends on the accommodation factor hence researchers [71,75] have suggested an alternative method[51] to calculate σ_v as

$$A_1(\sigma_v) = \frac{2 - \sigma_v}{\sigma_v} \left[A_1(1) - 0.1363(1 - \sigma_v) \right] \cdot \tag{17}$$

Here $A_1(1)$ is the first order slip coefficient computed for $\sigma_v = 1$. Maurer *et al.*[70] derived the accommodation factor σ_v based on A_1 as

$$\sigma_v = \frac{2}{A_1 + 1} \cdot \tag{18}$$

Similarly, second order von Smoluchowski's temperature-jump boundary conditions can be expressed as

$$T_s - T_w = \frac{2\gamma}{P_r(\gamma + 1)} \left[B_1 \lambda \left(\frac{\partial T}{\partial n} \right)_w + B_2 \lambda^2 \left(\frac{\partial^2 T}{\partial n^2} \right)_w \right] \cdot \tag{19}$$

Beskok's second order temperature jump condition [72] is as follows :

$$T_g = \frac{\left(\frac{(2-\sigma_T)}{\Pr}\right)\left(\frac{2\gamma}{(\gamma+1)}\right)T_\lambda + \sigma_T T_w}{\sigma_T + \left(\frac{(2-\sigma_T)}{\Pr}\right)\left(\frac{2\gamma}{(\gamma+1)}\right)}. \tag{20}$$

Table 3. Value of slip coefficients proposed in the literature for gas micro flows for σ_v =1.

Source	A_1	A_2
Maxwell,1879 [61]	1.0	0.0
Schamberg 1947 [76]	1.0	1.308 (5π/12)
Albertoni *et al*. 1963 [64]	1.1466	0.0
Cercignani[2] 1964 [50]	1.1466	0.647
Deissler[3], 1964 [69]	1.0	1.125 (9/8)
Sreekanth, 1969 [77]	1.1466	0.14
Loyalka *et al*., 1975 [51]	1.1466	0.0
Lang[4] ,1976 [78]	1.007	0.75
Hsia and Domoto, 1983 [80]	1.0	0.5
Loyalka and Hickey, 1989 [65]	1.1019	0.4490
Mitsuya, 1993 [81]	1.0	0.2222 (2/9)
Pan *et al*. 1999 [82]	1.125	0.0
Beskok[5], 2001 [72]	1.0	-0.5
Maurer *et al*., 2003 [70] (Helium)	1.2±0.05	0.23±0.1
Maurer *et al*., 2003 [70] (Nitrogen)	1.3±0.05	0.26±0.1
Cercignani *et al*. 2004 [30]	1.1366	0.6926
Lockerby *et al*.[6],2004 [62]	1.0	0.19 (6/10π)
Hadjiconstantinou[7], 2005 [83]	1.11	0.314
Dongari *et al*. [8],2007 [84]	1.4	0.7
Ewart *et al*. 2007 [71]	1.26±0.02	0.17±0.02
Struchtrup *et al*. 2008 [74]	1.0	0.5303 (5/3π)
Cercignani and Lorenzani 2010 [75]	1.209	0.2347

2.6 Treatment of slip flow based on effective viscosity

Another approach for extending the Navier-Stokes equation to transition regime is to consider the rarefaction effects in calculating the Navier-Stokes viscosity coefficient. In order to include the rarefaction effects Karniadakis *et al*. [85] proposed the following viscosity coefficient relationship

$$\frac{\mu(Kn)}{\mu} = \frac{1}{1+\alpha_g Kn}. \tag{21}$$

[2] After modification for hard sphere gas, refer Hadjiconstantinou [68] for details.

[3] Aubert and Colin [79] have also used Deissler's boundary conditions.

[4] $A_2 = 3\sigma_v / (4\Pr)$ for BGK model. For Maxwell gas, $A_2 = 1.125$

[5] $A_2 = -(2 - \sigma_v)/2\sigma_v$, where σ_v is the accommodation coefficient.

[6] $A_2 = \frac{9\Pr}{4\pi}\left(\frac{\gamma-1}{\gamma}\right)$, based on Maxwell-Burnett boundary condition.

[7] $A_2 = 0.31$ with Knudsen layer correction, $A_2 = 0.606$ without Knudsen layer correction.

[8] $A_1 = 1.0$, $A_2 = 0$ for $Kn \le 0.1$, $A_1 = 1.4$, $A_2 = 0.7$ for $0.1 < Kn \le 0.1$, $A_1 = 1.875$, $A_2 = 0.05$ for $1.0 < Kn$

Karniadakis *et al*. [85] uses only first order slip coefficient which is function of Knudsen number. While Roohi and Darbandi [86] have used second order slip formula coupled with viscosity coefficient correction evaluated using IP method expressed as

$$\frac{\mu(Kn)}{\mu} = \frac{1 + 0.75Kn + 19.98Kn^2}{1 + 0.89Kn + 4.70Kn^2}. \tag{22}$$

Fichman and Hetsroni [87] found that there is reduction in viscosity in the Knudsen layer due to interaction of molecules with the wall. This reduction of viscosity leads to an increase in slip velocity as a consequence of increase of the flow gradient in the direction normal to the wall. The effective viscosity proposed by Fichman and Hetsroni [87] is

$$\frac{\mu(\tilde{y}, \sigma_v)}{\mu} = \begin{cases} \sigma_v / 2 + (1 - \sigma_v)\tilde{y}, & \tilde{y} \le 1 \\ 1, & \tilde{y} > 1 \end{cases} \tag{23}$$

where $\tilde{y} = y/\lambda$, is the normal distance from the surface and λ is the mean free path. Fichman and Hetsroni [87] model fails to capture the asymptotic form of the velocity profile in the Knudsen layer near the surface[88]. Lilley and Sader [88] have shown that flow exhibits a striking power-law dependence on distance from the solid surface where the velocity gradient is singular i.e. the effective viscosity is zero, under arbitrary thermal accommodation. The effective viscosity proposed by Lilley and Sader [88] for $\tilde{y} < 1$ is

$$\frac{\mu(\tilde{y}, \sigma_v)}{\mu} = \frac{\tilde{y}^{1-\alpha(\sigma_v)}}{\alpha(\sigma_v)D(\sigma_v)}, \tag{24}$$

where $\alpha(\sigma_v)$ and $D(\sigma_v)$ are functions of momentum accommodation coefficient, σ_v, given in [88].

2.7 Treatment of slip flow based on Lattice Boltzmann method

The lattice Boltzmann (LB) method is a mesoscopic approach where details of the molecular motions are not required. Recently, Meng and Zhang [89] have shown that that the nine-velocity square lattice model D2Q9 model is not sufficient to capture flow characteristics in the Knudsen layer. Simulation of slip flows using LB method requires improvement in physics for high Knudsen flows to simulate nonlinear constitutive relations as well as proper method of slip boundary application. Researchers [90,91] have used diffuse reflection boundary condition simulated as the combination of the bounce-back and specular reflection boundary condition (similar to procedures developed in continuum kinetic theory) to simulate slip flows in LB method. There are broadly two approaches in LB method to include the effect of high Knudsen number : i) choice of discreet velocity set with sufficient symmetry so that the discreet moments approximates its counterpart based on continuous Boltzmann equation, ii) the second approach makes use of an effective relaxation time to capture the Knudsen layer. Sbragaglia and Succi [91] suggested suitable modification of the construction of the body force in the LB model in order to obtain the second-order slip. Kim *et al* [92] have implemented modification to the non-equilibrium energy flux to capture the slip phenomena up to second order in the Knudsen number. Guo *et al* [93] have used multiple effective relaxation times with wall confinement effects to simulate the Knudsen layer. The LB framework's extension to non-equilibrium flows still needs to evolve and mature to simulate transition regime [93]. The LB method are commonly used to simulate fluids with isothermal equations of state in a weakly compressible limit, it still needs development in the field of compressible high speed flows.

2.8 Treatment of slip flow based on Kinetic Flux Vector Splitting

We have adopted the approach of continuum solver coupled with slip boundary condition as it is computationally the least expensive. The slip flow simulation using the continuum solver can be carried out either by using slip models or by implementing kinetic wall boundary condition. It can be seen that there are large number of slip models existing in the literature, each with its own geometry specific slip coefficients and range of validity in Knudsen regime. Most of these slip models are for simple micro-channel flows. As described in Part 1 of the paper that even the first order slip model is not perfect as the slip velocity not only depends on the velocity gradient in the normal direction but also on the pressure gradient in the tangential flow direction. Researchers [94,95] have used Burnett equations coupled with slip models. For example Bao and Lin [95] have adopted Beskok's slip model [72]. Researchers [96-99] have used kinetic wall boundary condition obtained using the distribution function. Thus we require an approach which is computationally cheap and takes the slip velocity dependence on the fluid dynamic variations in the tangential direction. The approach also requires inclusion of the terms of order Kn^2 for its validity in the non-continuum slip bordering the transition region (Kn ≈ 0.1). In the present paper we have implemented slip boundary based on kinetic approach as described in Part 1 of the paper. The boundary condition at the surface of the solid object define the distribution function $f_1^{\Sigma}(v_x, v_y, v_z, I)$ of the reflected particles as a sum of diffuse and specular reflections. The state update based on KFVS implementation at the boundary after taking Ψ moment and writing in terms of inner product can be expressed as

$$U^{n+1} = U^n - \Delta t\left[\left(\frac{\partial GX^{\pm}}{\partial x}\right)^n + \left(\frac{\partial GY^{\pm}}{\partial y}\right)^n + \left(\frac{\partial GZ^{-}}{\partial z}\right)^n\right] \tag{25}$$

where

$$\left(\frac{\partial GX^{\pm}}{\partial x}\right)^n = \frac{\partial}{\partial x}\left(\int_{R^{\pm}}\int_{R}\int_{R^-}\int_{R^+}\Psi\left(\frac{v_x \pm \varphi|v_x|}{2}\right) f_1^{\Sigma} dv_x dv_y dv_z dI\right)^n \tag{26}$$

$$\left(\frac{\partial GY^{\pm}}{\partial y}\right)^n = \frac{\partial}{\partial y}\left(\int_{R}\int_{R^{\pm}}\int_{R^-}\int_{R^+}\Psi\left(\frac{v_y \pm \varphi|v_y|}{2}\right) f_1^{\Sigma} dv_x dv_y dv_z dI\right)^n \tag{27}$$

$$\left(\frac{\partial GZ^{-}}{\partial z}\right)^n = \frac{\partial}{\partial z}\left(\int_{R}\int_{R}\int_{R^-}\int_{R^+}\Psi v_z f_1^{\Sigma} dv_x dv_y dv_z dI\right)^n . \tag{28}$$

In above, U is the state vector and $GX^{\pm}$, $GY^{\pm}$ represents the split positive and negative octant fluxes and $GZ^{\pm}$ is the usual negative split flux resulting from the total distrbution $f_1^{\Sigma}(v_x, v_y, v_z, I)$ [100]. By using the higher order Chapman-Enskog distribution the kinetic treatment of slip can be extended to higher Knudsen number, Kn > 0.1 by adding the Burnett split flux terms. Full kinetic approach with the addition of Burnett split fluxes associated with second order Chapman-Enskog will make the computation quite costly. One of the simplest way to extend the KFVS based slip boundary condition is by further updating the slip velocity using the second order Kn^2 terms associated with the Burnett constitutive relations [62].

$$(u_s)^{n+1}_{2^{nd}\,Order} = (u_s)^{n+1}_{KFVS} + (\Delta u_s)^{n+1}_{Burnett} \tag{29}$$

The second order Kn^2 Burnett correction terms given by Lockerby *et al.* [62] is expressed as

$$\begin{aligned}(\Delta u_s)^{n+1}_{Burnett} = {} & \left(\frac{2-\sigma_v}{\sigma_v}\right)\lambda\left(2\frac{\mu}{\rho^2}\frac{\partial^2\rho}{\partial s\partial n} - \frac{\mu}{\rho T}\frac{\partial^2 T}{\partial s\partial n}\right)^n_w \\ & + \frac{3\,\mathrm{Pr}}{16\pi}\left(\frac{\gamma-1}{\gamma}\right)\lambda^2\left((45\gamma-61)\frac{\partial^2 u_s}{\partial s^2} + (45\gamma-49)\frac{\partial^2 u_n}{\partial s\partial n} - 12\frac{\partial^2 u_s}{\partial n^2}\right)^n_w .\end{aligned} \tag{30}$$

It should be noted that for polyatomic molecules this corrections requires a modification as Burnett coefficients are different. This Burnett correction to the slip velocity is under-relaxed by factor, *rf* which is below 0.1 such that

$$\left(\Delta u_s\right)_{Burnett}^{n+1} = \left(\Delta u_s\right)_{Burnett}^{n} + rf\left[\left(\Delta u_s\right)_{Burnett}^{n+1} - \left(\Delta u_s\right)_{Burnett}^{n}\right]. \tag{31}$$

3. VARIANCE REDUCTION KINETIC FLUX VECTOR SPLITTING FOR ROTATING FLOWS

Rossby number and Ekman number are the two dimensionless numbers characterizing the rotating flow. The Rossby number is defined as the ratio between the inertial and the Coriolis forces, and the Ekman number is defined as the ratio of the viscous forces to the Coriolis forces. To understand rotating flow one needs to understand the rotating frame of reference as compared to the inertial frame of reference. The Boltzmann equation can be solved in two reference frames: i) non-inertial frame i.e. frame rotating with the cylinders and ii) inertial frame i.e. in the laboratory frame in which the cylinders rotate. It should be noted that the relation between heat flux and temperature gradient, stress and velocity gradient is frame dependent [7]. In most of the rotational problems the secondary flow features are embedded in a primary rotating flow field. The variance reduction approach effectively captures the secondary flow feature (measured by Rossby number) embedded in a strongly rotating primary flow field.

3.1 Variance Reduction Kinetic Flux Vector Splitting (VRKFVS) for treatment for strong rotation

Validity of the Navier-Stokes equation as well as diffusion equation requires sufficient collision of particles and relaxation of the distribution to weak spatial gradients and slow temporal variations. There are cases when gradients are substantial on the scale of mean free path or temporal changes are relatively rapid compared to mean collision time. Causality is violated, since the particle flux is obviously limited by the finite particle speed. One way to proceed is to use Boltzmann equation which is strictly causal by taking higher moments with appropriate closure relations. Investigation revealed that the shear stress depends on the shear amplitude as it reaches a maximum and then decreases as the velocity gradient increases. It should be noted that the shear amplitude for the non-inertial rotational problem should be observed in the correct frame of reference with variance reduction approach. In the variance reduction approach Boltzmann equation is written as a perturbation from its state of equilibrium [17,18]. Gas under isothermal condition with temperature $T = T_0$ uniformly rotating with angular velocity ω in a cylinder of radius r_{wall} can be described by rigid body rotation [3]. The flow variables with rigid body condition are expressed as

$$\left[v_z, v_r, v_\theta,\ T, \rho\right]_{RB} \equiv \left[0, 0, \omega\ r, T_o, \rho_{wall} exp\left(\frac{\omega^2}{2RT_o}(r^2 - r_{wall}^2)\right)\right] \tag{32}$$

where the subscript $_{RB}$ denotes the state of rigid body rotation. Boltzmann equation observed in the rigid body rotational frame leads to a very interesting result as velocity distribution associated with the rigid body solution satisfies both the inviscid as well as viscous solution. The velocity distribution associated with this rigid body rotation, f_{RB} is a Maxwellian. This variant of BGK-Boltzmann equation is then expressed in the variance reduction form as

$$\frac{\partial(\Delta f)}{\partial t} + \frac{\partial \vec{v}\left(\Delta f_1\right)}{\partial \vec{x}} = 0 \quad or \quad \frac{\partial\left(\Delta \hat{f}\right)}{\partial t} + \frac{\partial \vec{v}\left(\Delta f_1\right)}{\partial \vec{x}} = 0 \tag{33}$$

where $\Delta f_1 = \Delta f + Kn\ \Delta \bar{f}_1$, $\Delta f = f_0 - f_{RB}$, $\Delta \bar{f}_1 = \bar{f}_1 - \bar{f}_1^{RB}$ and $\Delta \hat{f} = f_1 - f_{RB}$ with $Kn\Delta \bar{f}_1$ expressed as

$$Kn\Delta \bar{f}_1 \approx -t_R\left[\frac{\partial \Delta f}{\partial t} + \nabla_{\vec{x}}.(\vec{v}\Delta f)\right]. \tag{34}$$

The steep gradients observed in stationary inertial frame now appear to be a weak perturbation. Taking ψ moments of the resulting variant of Boltzmann equation leads to upwind Navier-Stokes equation based on Variance Reduction Kinetic Flux Vector Splitting (VRKFVS) form as

$$\frac{\partial}{\partial t}(U-U_{RB})+\frac{\partial}{\partial x}\left[\left(GX_I^{\pm}\right)-\left(GX_I^{\pm}\right)_{RB}+\left(GX_V^{\pm}\right)_{\Delta}\right]+\frac{\partial}{\partial y}\left[\left(GY_I^{\pm}\right)-\left(GY_I^{\pm}\right)_{RB}+\left(GY_V^{\pm}\right)_{\Delta}\right] \\ +\frac{\partial}{\partial z}\left[\left(GZ_I^{\pm}\right)-\left(GZ_I^{\pm}\right)_{RB}+\left(GZ_V^{\pm}\right)_{\Delta}\right]=0 \tag{35}$$

where U_{RB} is the state update vector , $(GX_I^{\pm})_{RB}$, $(GY_I^{\pm})_{RB}$ and $(GZ_I^{\pm})_{RB}$ are the split fluxes based on rigid body rotation. The viscous fluxes $(GX_V^{\pm})_{\Delta}$, $(GY_V^{\pm})_{\Delta}$ and $(GZ_V^{\pm})_{\Delta}$ are computed based on relative velocity field over the rigid body rotation. Rossby number which gives relative importance of inertial with respect to Coriolis forces is also a measure of departure from the rigid body solution. Solution for the small perturbation from the rigid body rotation can be obtained in terms of Rossby number, $\varepsilon=\frac{\Delta\omega}{\omega}$ [3]. We have defined the local Rossby number, ε based on z-component of vorticity vector Ω_z as

$$\varepsilon=\left|1-\frac{\Omega_z}{(\Omega_z)_{RB}}\right|. \tag{36}$$

This local Rossby number is used as a measure of departure from the rigid body solution, for example if $\varepsilon<\varepsilon_s$ solver switches to this special form of Navier-Stokes equations based on VRKFVS. Mahendra *et al.*[18] based on numerical experiments have observed accuracy with $\varepsilon_s = 0.1$.

3.2 Continuum breakdown in rotating flow field

Rossby number, ε can also be defined as the deviation from equilibrium rigid body rotation, expressed as

$$\varepsilon=\frac{\int_{R^N}\int_{R^+}\psi_i(f_1-f_0)\,d\vec{v}\,dI}{\int_{R^N}\int_{R^+}\psi_i f_0\,d\vec{v}\,dI} \tag{37}$$

where moment variable $\psi_i\in\Psi\equiv\{1,\vec{v},\vec{v}^T\vec{v}\}$ or any other admissible $\psi_i\in\Psi\equiv\{1,\vec{v},\vec{v}\otimes\vec{v},\cdots\}$. f_0 is Maxwellian distribution function and f_1 is the Chapman-Enskog distribution function corresponding to the Navier-stokes equation.

The local Knudsen number for a rotating flow field based on the degree of departure from the non-equilibrium flow state will then be a function of Rossby number, ε as follows

$$Kn=\frac{\int_{R^N}\int_{R^+}\psi_i(f-f_1)\,d\vec{v}\,dI}{\varepsilon\int_{R^N}\int_{R^+}\psi_i f_0\,d\vec{v}\,dI} \tag{38}$$

where f is a higher order distribution function.

4. MODIFIED SPLIT-STENCIL LEAST SQUARE KINETIC UPWIND METHOD FOR NAVIER-STOKES

For carrying out numerical simulation of Navier-Stokes equations for complex multibody configuration with many components the generation of suitable grid becomes the bottleneck. Conventional approach requires grids which include structured multi-block meshes, chimera or overset grids, unstructured grids, Cartesian grids and hybrid grids [17]. Recently meshfree or meshless methods have gained popularity. All meshless numerical methods share a common feature that no mesh is needed and the solver is capable of operating on an arbitrary distribution of points. Smooth Particle Hydrodynamics

(SPH), Reproducing Kernel Particle Method (RKPM), Moving Least-Square Reproducing Kernel Method, Least Square Kinetic Upwind Method (LSKUM), Element Free Galerkin Method (EFG), h-p-Clouds, Partition of Unity Finite Element Method, etc [17] are some of the methods belonging to this family of meshless methods. In the present meshless solver the points are generated around each component of the multibody configuration using simple grid generator and then the points around each components are merged to form the cloud of points. Meshless method in this case requires cloud of points and its connectivity.

4.1 Pre-processing for multi-body configuration

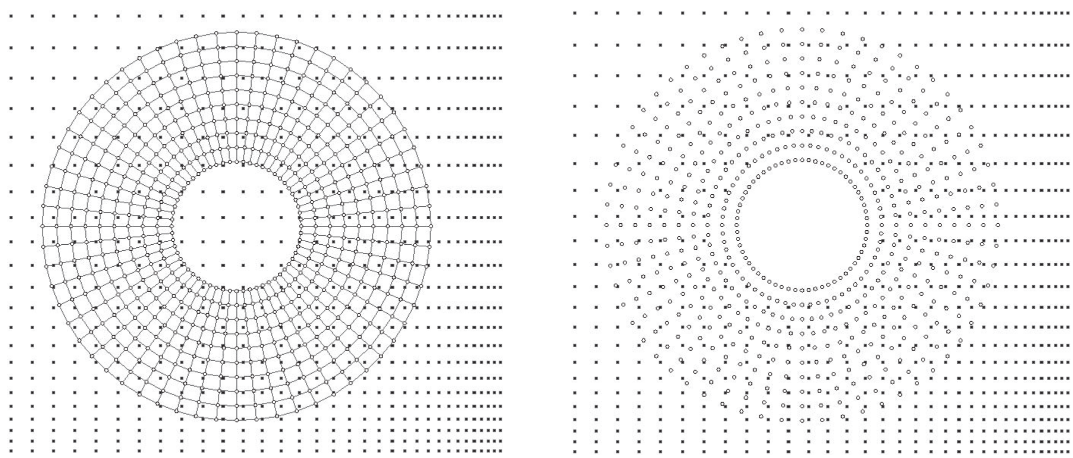

Figure 2. Pre-processing of cloud of points

The task of generating suitable grid for a complex multi-body configuration can be accomplished by breaking down a geometrically complex object as a union of several geometrically simple objects, generating grid around each simple object and then finally merging all the grid points into a *cloud* of points enveloping the complex multi-body configuration. We need an appropriate pre-processor to carry out merging of points and then generating connectivity. Let us define nodes generated around simple objects as *sub-clouds* that will merge to form the cloud.

For example define sub-clouds around a circle shaped body as α sub-cloud which is to be merged with background β sub-cloud. A pre-processor is required to merge many sub-clouds as shown in Figure 2. The union of two sub-clouds can be written as

$$sC(\alpha) \cup sC(\beta) = sC(\alpha) + sC(\beta) - sC(\alpha) \cap sC(\beta) - sC^C(\alpha) - sC^C(\beta) \tag{39}$$

where

$$sC(\alpha) \cap sC(\beta) = \left\{\forall P_i : P_i \in sC(\alpha), \forall P_j : P_j \in sC(\beta) \ \exists\, d(P_i, P_j) \le h_{\min}\right\} \tag{40}$$

$$sC^C(\alpha) = \{\forall P_i : P_i \mid P_i \notin sC(\alpha), P_i \in Bc(\alpha)\} \tag{41}$$

$$sC^C(\beta) = \{\forall P_i : P_i \mid P_i \notin sC(\beta), P_i \in Bc(\beta)\}\,. \tag{42}$$

The term $sC(\alpha) \cap sC(\beta)$ denote nodes belonging to sub-clouds $sC(\alpha)$ of object α and sub-cloud of $sC(\beta)$ object β which are very close to each other i.e. within the tolerance $h_{\min}$ specified by the user. While $Bc(\alpha)$ and $Bc(\beta)$ denote blank nodes i.e. nodes which will perform no computation. $Bc(\alpha)$ can also be defined as a set of sub-clouds lying inside the body or in any other non-computing domain of α and similarly $Bc(\beta)$ can be defined as a set of sub-clouds lying inside the body or in any other non-computing domain of β. Thus, the term $sC^c(\alpha)$ and $sC^c(\beta)$ denote the set of all the nodes which do not belong to sub-clouds sC(α), sC(β) and these nodes lie inside the body or in any other non-computing domain of α and β respectively. The term $sC(\alpha) \cup sC(\beta)$ denotes the merging phase where the nodes that lie inside the body or in any other non-computing domain are deleted by ray-tracing algorithm. The merging phase also deletes the nodes based on the criterion $d(P_i, P_j) \leq h_{\min}$. The parameter $d(P_i, P_j)$ gives the Euclidean distance between P_i and P_j.

4.2 Meshless solver m-SLKNS

The present meshless solver is a modified form of Split-Stencil least square kinetic upwind method for Navier-Stokes (SLKNS) [18]. SLKNS splits the set of neighbours (also defined as connectivity, $N(P_0) = \{\forall P_i : d(P_0, P_i) < h\}$ for node P_0) so as to capture the viscous flow features while enforcing upwinding. Let ϕ be any function of x, y and z and further it is assumed that it is given at all nodes i.e. it is given at all points in a cloud. We are interested in finding the derivatives of ϕ at all the nodes. The derivatives are obtained in the following way. Consider a point o surrounded by n points then error at any point in the neighbourhood of o gives us,

$$ex_i = \frac{(\phi_i)_{exact} - \phi_i}{\Delta x_i} = \frac{\Delta \phi_i}{\Delta x_i} - \phi_{xo} - \frac{\Delta y_i}{\Delta x_i}\phi_{yo} - \frac{\Delta z_i}{\Delta x_i}\phi_{zo} + O(\Delta x, \frac{(\Delta y)^2}{\Delta x}, \frac{(\Delta z)^2}{\Delta x}) \quad for \quad i = 1, \cdots, nx \tag{43}$$

$$ey_i = \frac{(\phi_i)_{exact} - \phi_i}{\Delta y_i} = \frac{\Delta \phi_i}{\Delta y_i} - \frac{\Delta x_i}{\Delta y_i}\phi_{xo} - \phi_{yo} - \frac{\Delta z_i}{\Delta y_i}\phi_{zo} + O(\frac{(\Delta x)^2}{\Delta y}, \Delta y, \frac{(\Delta z)^2}{\Delta y}) \quad for \quad i = 1, \cdots, ny \tag{44}$$

$$ez_i = \frac{(\phi_i)_{exact} - \phi_i}{\Delta z_i} = \frac{\Delta \phi_i}{\Delta z_i} - \frac{\Delta x_i}{\Delta z_i}\phi_{xo} - \frac{\Delta y_i}{\Delta z_i}\phi_{yo} - \phi_{zo} + O(\frac{(\Delta x)^2}{\Delta z}, \frac{(\Delta y)^2}{\Delta z}, \Delta z) \quad for \quad i = 1, \cdots, nz \tag{45}$$

where $\Delta x_i = x_i - x_o$, $\Delta y_i = y_i - y_o$, $\Delta z_i = z_i - z_o$ and $\Delta\phi_i = \phi_i - \phi_o$. Finding the derivative at point o is a least squares problem where error norm is to be minimized with respect to ϕ_{xo}, ϕ_{yo} and ϕ_{zo} using stencil $N(P_o)$. Most of least square approaches use the normal equations approach to find $\Phi_o = [\phi_{xo}, \phi_{yo}, \phi_{zo}]^T \in \mathrm{R}^n$ such that $\| A_N \Phi_o - \Delta\phi_N \|_2$ is minimized where data matrix $A_N \in \mathrm{R}^{n \times m}$ and observation $\Delta\phi_N = [\Delta\phi_1, \Delta\phi_2, \ldots, \Delta\phi_m]^T \in \mathrm{R}^m$ where subscript $_N$ denotes stencil $N(P_o)$. Whereas, modified SLKNS (m-SLKNS) minimizes $\Sigma\|ex\|_2$, $\Sigma\|ey\|_2$ and $\Sigma\|ez\|_2$ with respect to ϕ_{xo}, ϕ_{yo} and ϕ_{zo} respectively for each carefully selected sub-stencils $N_x(P_o)$, $N_y(P_o)$ and $N_z(P_o)$ with nx, ny and nz points or nodes . Thus, m-SLKNS is similar to SLKNS as the basic stencil $N(P_0)$ gets divided into 6 different kind of upwind sub-stencils: $N_x^+(P_o)$, $N_x^-(P_o)$, $N_y^+(P_o)$, $N_y^-(P_o)$, $N_z^+(P_o)$ and $N_z^-(P_o)$ are defined by connectivity parameters as follows.

$$\begin{aligned} N_x^+(P_o) &= \left\{ P_i \in N_x(P_o) : \Delta x_i \leq 0, \frac{\Delta y_i}{\Delta x_i} \leq 1, \frac{\Delta z_i}{\Delta x_i} \leq 1 \right\}, \\ N_x^-(P_o) &= \left\{ P_i \in N_x(P_o) : \Delta x_i \geq 0, \frac{\Delta y_i}{\Delta x_i} \leq 1, \frac{\Delta z_i}{\Delta x_i} \leq 1 \right\} \end{aligned} \tag{46}$$

$$\begin{aligned} N_y^+(P_o) &= \left\{ P_i \in N_y(P_o) : \Delta y_i \leq 0, \frac{\Delta x_i}{\Delta y_i} \leq 1, \frac{\Delta z_i}{\Delta y_i} \leq 1 \right\}, \\ N_y^-(P_o) &= \left\{ P_i \in N_y(P_o) : \Delta y_i \geq 0, \frac{\Delta x_i}{\Delta y_i} \leq 1, \frac{\Delta z_i}{\Delta y_i} \leq 1 \right\} \end{aligned} \tag{47}$$

$$\begin{aligned} N_z^+(P_o) &= \left\{ P_i \in N_z(P_o) : \Delta z_i \leq 0, \frac{\Delta x_i}{\Delta z_i} \leq 1, \frac{\Delta y_i}{\Delta z_i} \leq 1 \right\}, \\ N_z^-(P_o) &= \left\{ P_i \in N_z(P_o) : \Delta z_i \geq 0, \frac{\Delta x_i}{\Delta z_i} \leq 1, \frac{\Delta y_i}{\Delta z_i} \leq 1 \right\} \end{aligned}. \tag{48}$$

To illustrate the derivative calculation consider ϕ to be any function of x, y in two-dimensions with cloud of points and split stencils $N_x(P_o)$ and $N_y(P_o)$ bounded within a 45 degree line as shown in Figure 3. Let us define error for any point P_i based on Taylor series around P_o for ϕ as

$$ex_i = \frac{(\phi_i)_{exact} - \phi_i}{\Delta x_i} = \left(\Delta\phi_i - \phi_{xo} - \frac{\Delta y_i}{\Delta x_i}\phi_{yo}\right) + O(\Delta x,, \frac{(\Delta y)^2}{\Delta x}) \text{ for connectivity set } N_x\ (P_o) \tag{49}$$

$$\text{and } ey_i = \frac{(\phi_i)_{exact} - \phi_i}{\Delta y_i} = \left(\Delta\phi_i - \frac{\Delta x_i}{\Delta y_i}\phi_{xo} - \phi_{yo}\right) + O(\frac{(\Delta x)^2}{\Delta y},\ \Delta y) \text{ for connectivity set } N_y\ (P_o)\cdot \tag{50}$$

Thus we have two sets of the square of error $\Sigma\|ex\|_2$ and $\Sigma\|ey\|_2$ defined as

$$\sum\|ex\|_2 = \sum_{i=1}^{nx}\left(\frac{\Delta\phi_i}{\Delta x_i} - \phi_{xo} - \phi_{yo}\frac{\Delta y_i}{\Delta x_i}\right)^2 = \sum_{i=1}^{nx}\left(\frac{\Delta\phi_i}{\Delta x_i} - \phi_{xo} - \phi_{yo}\eta_i\right)^2 \tag{51}$$

$$\sum\|ey\|_2 = \sum_{i=1}^{ny}\left(\frac{\Delta\phi_i}{\Delta y_i} - \phi_{xo}\frac{\Delta x_i}{\Delta y_i} - \phi_{yo}\right)^2 = \sum_{i=1}^{ny}\left(\frac{\Delta\phi_i}{\Delta y_i} - \phi_{xo}\frac{1}{\eta_i} - \phi_{yo}\right)^2 \tag{52}$$

where slope $\eta_i = \frac{\Delta y_i}{\Delta x_i}\phi\cdot$

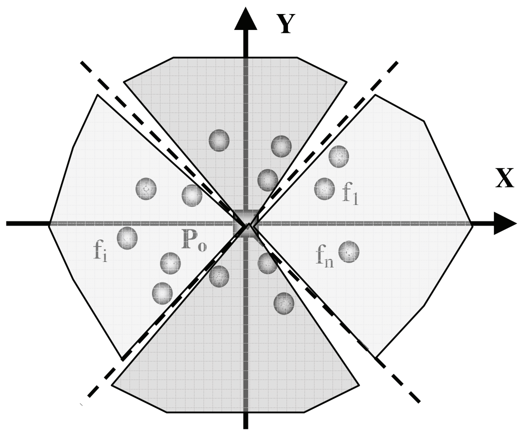

Figure 3. Typical split connectivity around point Po

Minimizing the sum of the squares of error $\Sigma\|ex\|_2$ and $\Sigma\|ey\|_2$ with respect to ϕ_{xo} and will ϕ_{yo} lead to $C\Phi_o = \Delta\Phi_{xy}$ where

$$C = \begin{bmatrix} 1. & \frac{1}{nx}\sum_{i=1}^{nx}\eta_i \\ \frac{1}{ny}\sum_{i=1}^{ny}(\eta_i)^{-1} & 1. \end{bmatrix}, \Phi_o = \begin{bmatrix}\phi_{xo} \\ \phi_{yo}\end{bmatrix} \text{ and } \Delta\Phi_{xy} = \begin{bmatrix} \frac{1}{nx}\sum_{i=1}^{nx}\frac{\Delta\phi_i}{\Delta x_i} \\ \frac{1}{ny}\sum_{i=1}^{ny}\frac{\Delta\phi_i}{\Delta y_i}\end{bmatrix}. \tag{53}$$

The derivatives ϕ_{xo} and ϕ_{yo} can be obtained as

$$\phi_{xo} = \frac{\frac{1}{nx}\sum_{i=1}^{nx}\frac{\Delta\phi_i}{\Delta x_i} - \left(\frac{1}{nx}\sum_{i=1}^{nx}\eta_i\right)\left(\frac{1}{ny}\sum_{i=1}^{ny}\frac{\Delta\phi_i}{\Delta y_i}\right)}{1. - \left(\frac{1}{nx}\sum_{i=1}^{nx}\eta_i\right)\left(\frac{1}{ny}\sum_{i=1}^{ny}(\eta_i)^{-1}\right)} \text{ and}$$

$$\phi_{yo} = \frac{\frac{1}{ny}\sum_{i=1}^{ny}\frac{\Delta\phi_i}{\Delta y_i} - \left(\frac{1}{ny}\sum_{i=1}^{ny}\frac{1}{\eta_i}\right)\left(\frac{1}{nx}\sum_{i=1}^{nx}\frac{\Delta\phi_i}{\Delta x_i}\right)}{1. - \left(\frac{1}{nx}\sum_{i=1}^{nx}\eta_i\right)\left(\frac{1}{ny}\sum_{i=1}^{ny}(\eta_i)^{-1}\right)}. \tag{54}$$

Two eigen values of matrix C are

$$\lambda_e^{\pm} = 1 \pm \sqrt{\frac{1}{nx}\sum_{i=1}^{nx}\eta_i \frac{1}{ny}\sum_{i=1}^{ny}(\eta_i)^{-1}} \quad . \tag{55}$$

If the chosen split connectivity stencils $N_x\ (P_o)$ and $N_y\ (P_o)$ are bounded within a 45 degree line then in such case $\eta_i \le 1$ for $N_x\ (P_o)$ and $(\eta_i)^{-1} \le 1$ for $N_y\ (P_o)$, thus the matrix C is always well-conditioned. Advantage of this method is its low storage requirement as we are only storing the off diagonal terms of the matrix C. The second advantage is for each sub-stencils we can assign separate weights based on geometry or gradients.

The modified KFVS for Navier-Stokes for 3-D geometries [17,18] can be derived by using Courant splitting at the Boltzmann level as

$$\begin{aligned}
&\left\langle \Psi, \frac{\partial f_1}{\partial t}\right\rangle + \left\langle \Psi, \frac{v_x + \varphi|v_x|}{2}\frac{\partial f_1}{\partial x}\right\rangle_{N_x^+(P_o)} + \left\langle \Psi, \frac{v_x - \varphi|v_x|}{2}\frac{\partial f_1}{\partial x}\right\rangle_{N_x^-(P_o)} \\
&+ \left\langle \Psi, \frac{v_y + \varphi|v_y|}{2}\frac{\partial f_1}{\partial y}\right\rangle_{N_y^+(P_o)} + \left\langle \Psi, \frac{v_y - \varphi|v_y|}{2}\frac{\partial f_1}{\partial y}\right\rangle_{N_y^-(P_o)} \\
&+ \left\langle \Psi, \frac{v_z + \varphi|v_z|}{2}\frac{\partial f_1}{\partial z}\right\rangle_{N_z^+(P_o)} + \left\langle \Psi, \frac{v_z - \varphi|v_z|}{2}\frac{\partial f_1}{\partial z}\right\rangle_{N_z^-(P_o)} = 0 \quad .
\end{aligned} \tag{56}$$

$\Psi = \left[1, \vec{v}, I + \frac{1}{2}\vec{v}^T\vec{v}\right]^T$ and the dissipation control factor, $\varphi = \varphi\ (\rho/\varepsilon)$ is the function of the local Rossby number and density. Ψ moment leads to split flux Navier-Stokes state update equations as follows

$$U^{n+1} = U^n - \Delta t \begin{bmatrix} \left(\frac{\partial GX^+}{\partial x}\right)^n_{N_x^+(P_o)} + \left(\frac{\partial GX^-}{\partial x}\right)^n_{N_x^-(P_o)} \\ + \left(\frac{\partial GY^+}{\partial y}\right)^n_{N_y^+(P_o)} + \left(\frac{\partial GY^-}{\partial y}\right)^n_{N_y^-(P_o)} \\ + \left(\frac{\partial GZ^+}{\partial z}\right)^n_{N_z^+(P_o)} + \left(\frac{\partial GZ^-}{\partial z}\right)^n_{N_z^-(P_o)} \end{bmatrix} . \tag{57}$$

$GX^{\pm}$, $GY^{\pm}$ and $GZ^{\pm}$ represent the split inviscid and viscous fluxes. Viscous fluxes are upwinded and treated similar to inviscid fluxes. Second order accuracy in SLKNS is acheived through a two-step procedure similar to one used in LSKUM described in [101], this when coupled with inner iterations leads to second order of accuracy.

5. RESULTS AND DISCUSSIONS

The meshless solver m-SLKNS was validated with variety of test cases. First two test case consists of continuum supersonic and transonic flow over NACA0012 aerofoil chosen to validate the meshless solving capability of the m-SLKNS solver. Third test case of velocity distribution in cylindrical annuli was chosen to validate the diffuse reflection slip boundary condition. Fourth validation test case is a well known velocity inversion behavior observed for rarefied flows chosen to test the axi-symmetric solving capability of the solver. The fifth validation case is the simulation of rarefied flow in a rotating eccentric cylinder. This test case validates the slip modeling abilities of the solver under condition of rarefaction and adverse pressure gradient. The sixth case is the flow field around a stationary body in the rotating subsonic and supersonic flow field. Solver m-SLKNS captures the vortex in the sub-sonic rarefied pocket ahead of the stationary body under supersonic flow conditions.

5.1 Supersonic viscous flow over NACA0012 aerofoil

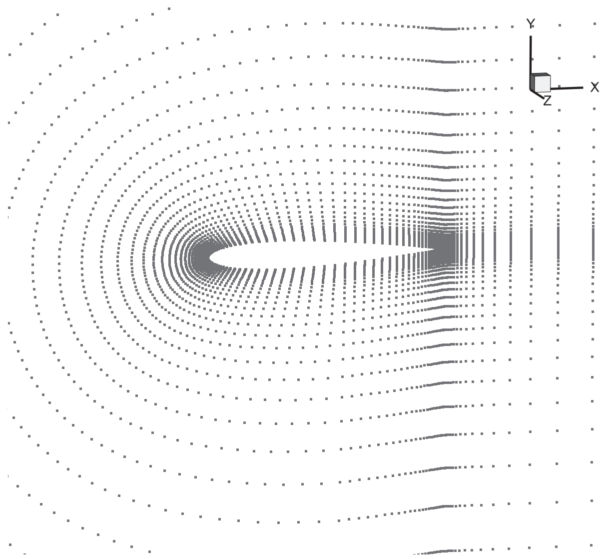

Figure 4. Cloud of points around NACA0012 aerofoil

This validation test consists of free stream supersonic flow at M_∞=*1.5* past a NACA0012 aerofoil at an angle of attack α=*0*$^\circ$. The Reynolds number based on the aerofoil chord is *10000*. Total *10143* cloud of points was generated using C-type mesh of size *207×49* shown in Figure 4. The computation reveals a fish tail shock shown in Figure 5.

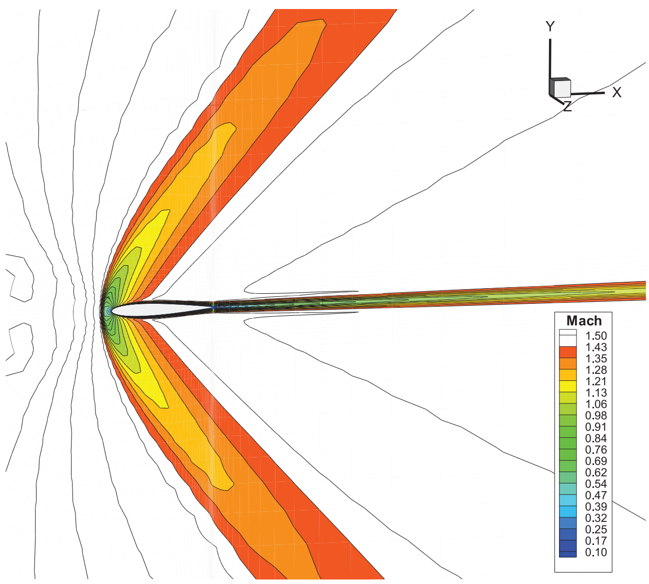

Figure 5. Mach contours

5.2 Transonic viscous flow over NACA0012 aerofoil

This test consists of free stream transonic flow at M_∞=*0.8* past a NACA0012 aerofoil at an angle of attack α=*10*$^\circ$. The Reynolds number based on the aerofoil chord is *500*. Figure 6 shows the Mach contours with two counter rotating vortex. Figure 7 shows the coefficient of friction plot which compares well with the results of SLKNS code [18], Fortunato and Magi [102] and Catalano *et al.*[103].

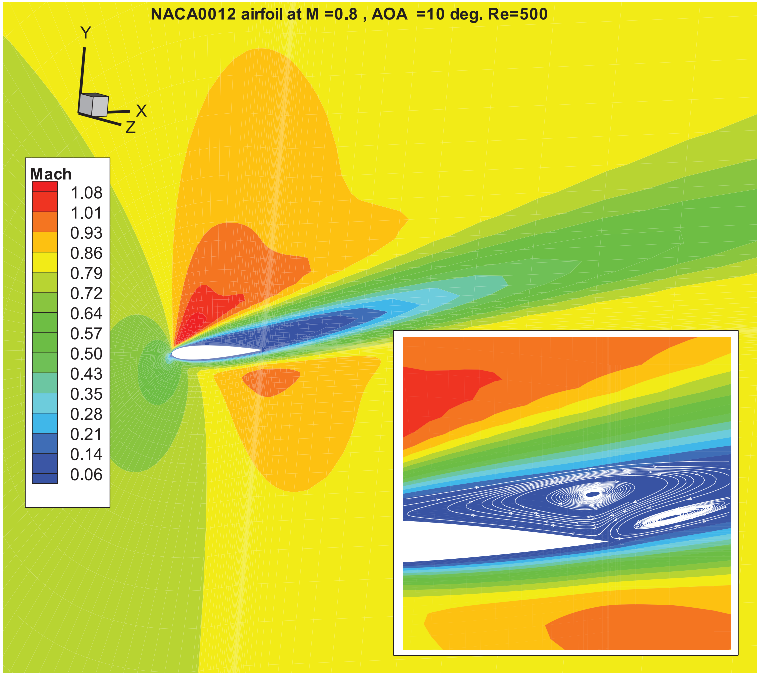

Figure 6. Mach contours with zoomed view showing streamlines in the region of flow separation.

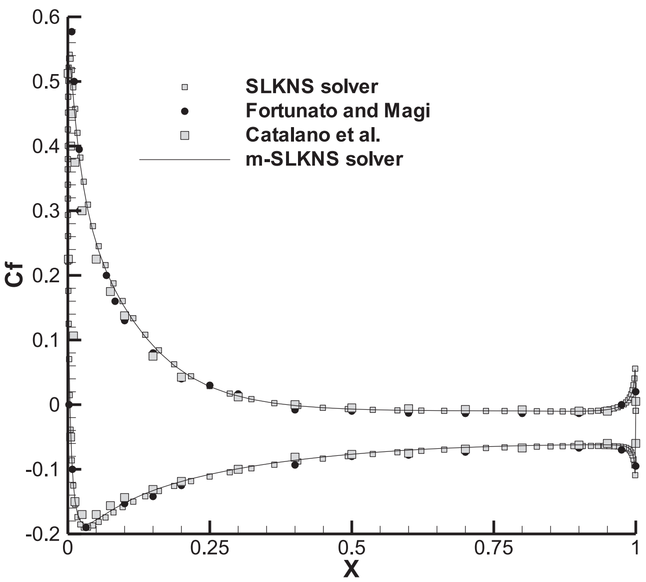

Figure 7. Plot of coefficient of friction

5.3 Slip flow in an annulus

Avci and Aydin [104] investigated laminar slip flow in a micro-annulus between two concentric cylinders of inner radius r_i and r_o outer radius. Avci and Aydin [104] considered a slip flow with fully diffuse reflection and found out a relationship in terms of dimensionless radius $r_d = r_i/r_o$ for dimensionless velocity distribution as

$$\frac{V_Z}{V_{Zmax}} = \frac{2\left[1-\left(\frac{r}{r_o}\right)^2 + r_m^2 \ln\left(\frac{r}{r_o}\right) + A\right]}{B} \tag{58}$$

where A, B and r_m are, respectively given as

$$\begin{aligned} A &= 4Kn(1-r_d)(1-r_m^2) \\ B &= \left[1-r_d^2 - 4r_m^2\left(\frac{1}{2}+\frac{r_d^2}{1-r_d^2}\ln(r_d)\right)+2A\right] \\ r_m &= \left[\frac{(1-r_d^2)(1+4Kn)}{2\ln(\frac{1}{r_d}) - 4Kn(\frac{r_d^2-1)}{r_d^2}}\right]^{1/2} \end{aligned} \tag{59}$$

Here Knudsen number, Kn is defined with respect to hydraulic diameter, d_h of the annuli as

$$Kn = \frac{\lambda}{d_h} = \frac{\lambda}{2(r_o - r_i)} \tag{60}$$

In this test case we considered cylindrical annuli with inner radius of *0.02* m and outer radius of *0.1* m with argon flowing at an average pressure of *2* Pa. The solver m-SLKNS was run for slip flow case at Kn = 0.0227. Figure 8 shows the plot of dimensionless velocity which compares well with the analytical results of Avci and Aydin[104] based on Maxwell's velocity slip boundary condition.

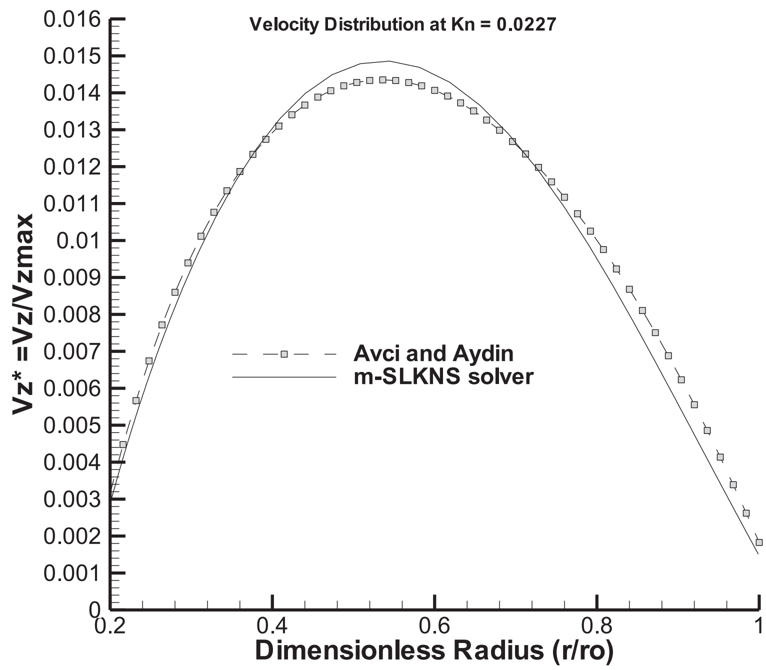

Figure 8. Velocity distribution

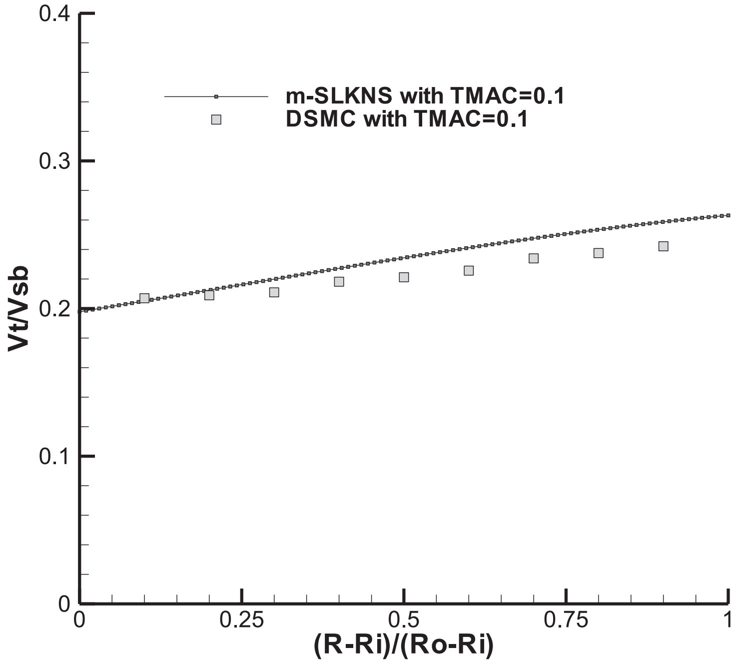

Figure 9.Velocity inversion

5.4 Velocity inversion

Couette flow between concentric inner rotating and outer stationary cylinders is one of a classical fluid dynamics problem. However, under certain condition of rarefaction and wall (when accommodation coefficient is small), the velocity profile inverts i.e. the gas rotates faster near the stationary wall. This phenomenon was first predicted by Einzel *et al* [105]. Many researchers [62,106,107] have carried out analytical and DSMC studies to explain this anomalous behavior. In this test case Argon gas is confined between inner and outer cylinder that have tangential momentum accommodation coefficient of *0.1* and radii of 3λ and 5λ respectively, where mean free path, $\lambda = 6.25 \times 10^{-8}$m. Inner cylinder rotates with angular speed, $\omega = 5.17 \times 10$ rad/s and outer cylinder is held stationary[106]. Meshless solver m-SLKNS was able to capture this anomalous behaviour of velocity inversion. Figure 9 shows the plot of the non-dimensional tangential velocity with respect to non-dimensional radial distance for m-SLKNS and DSMC.

From physical point of view the rotating cylinder imparts the circumferential momentum to the molecules undergoing diffuse reflection. At smaller Knudsen number most of the momentum transfer is due to molecular collisions. When the outer cylinder is specularly reflecting then no circumferential momentum is transferred to the outer cylinder [107]. As a consequence the gas accelerates and reaches the stationary state of rigid body rotation (the distribution function is a Maxwellian), satisfying the Onsager's principle of least dissipation of energy valid for processes close to equilibrium.

5.5 Rarefied flow in a rotating eccentric cylinders

The flow confined between two eccentric cylinders is much more complex than the axisymmetric case. This flow even though confined within such a simple geometry generates myriad nonlinearities associated with the Navier-Stokes equation. Consider a flow of argon confined between outer rotating and inner stationary eccentric isothermal cylinders. Researchers [108,109] have given approximate closed form solution to describe such a flow, others have used approximate analytical solutions by either using an eccentricity parameter [110] or the Reynolds number [111]. Numerical techniques were also developed [112-114] to simulate continuum flows for this eccentric geometry. Socio and Marino [115,116] studied this problem using direct simulation Monte-Carlo (DSMC) and carried out detailed study by taking effects of eccentricity and different wall rotational speed for different gas rarefaction for wide range of Knudsen number. Let r_0 be the outer radius and r_i be the inner radius. The Knudsen number is defined as

$$Kn = \frac{\lambda}{(r_o - r_i)} \cdot \tag{61}$$

Total *14962* points were taken for this particular case for validating m-SLKNS solver using VRKFVS scheme. Figure 10 shows the cloud of points and figure 11 shows the region of continuum breakdown based on gradient length Knudsen number. Numerical simulation for eccentricity of *0.45* at Mach = *0.5* for Kn = *0.0175* and Kn = *0.1* was carried out with isothermal wall held at temperature of *300* deg. K. Figure 12 shows the plot of local Knudsen number contours for Kn = *0.0175*. Figure 13 reveals contours of temperature similar to observed in DSMC for the case with Kn = *0.1*. In this case the maximum temperature observed is *308.82* deg. K and minimum temperature is *293.21* deg. K using m-SLKNS solver based on VRKFVS scheme. Thus, maximum temperature ratio is *1.029* and minimum temperature ratio is *0.977*. Socio and Marino[116] have observed maximum temperature ratio as *1.033* and minimum at *0.979* using DSMC. Simulation revealed that the onset of vortex was being helped by the eccentricity while gas rarefaction had an opposite influence in subsidence of the vortex. The vortex for eccentricity of *0.45* at Mach = *0.5* subsides at much lower Kn = *0.72*, this does not compare well with the results of Kn = *1.0* by Socio and Marino [116]. One of the reasons of disagreement might be the extension of the present kinetic based boundary to higher Knudsen number flow using corrections with Kn^2 order Burnett terms. It should be noted that Socio and Marino [115,116] employed the bi-polar coordinate system to simplify the geometric representation at the cost of complications introduced due to the rectilinear trajectories of the particles. The density contour plot reveals the density rises exponentially towards the periphery. The bipolar coordinate system used in DSMC leads to large size cells towards the rotating peripheral region where density rises sharply. While in m-SLKNS solver the cloud of points were more clustered radially towards the peripheral wall as well as in the azimuthal region.

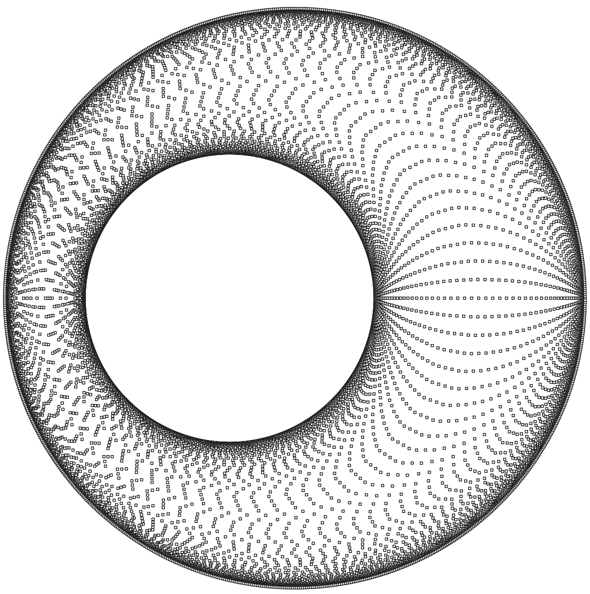

Figure 10. Cloud of points

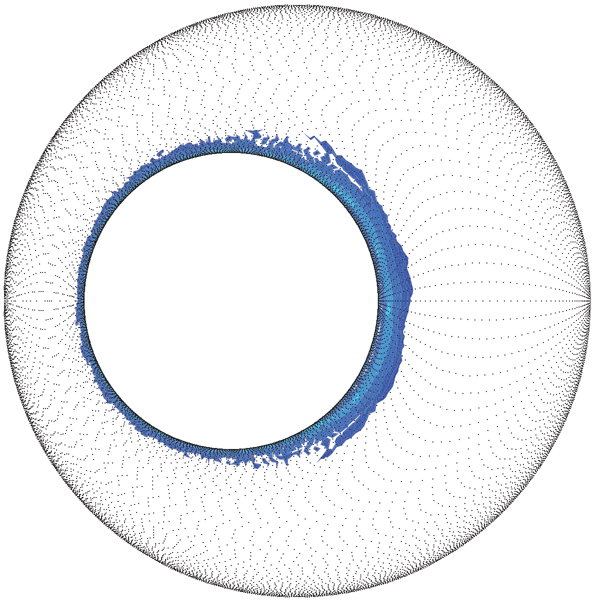

Figure 11. Shaded portion shows the region of Navier-Stokes breakdown

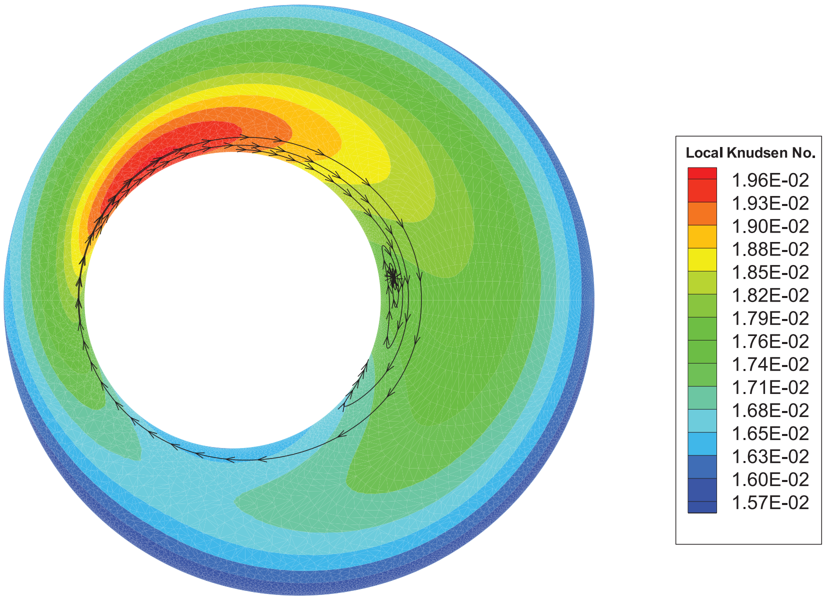

Figure 12. Plot of local Knudsen number with region showing separation of flow at Kn=0.0175

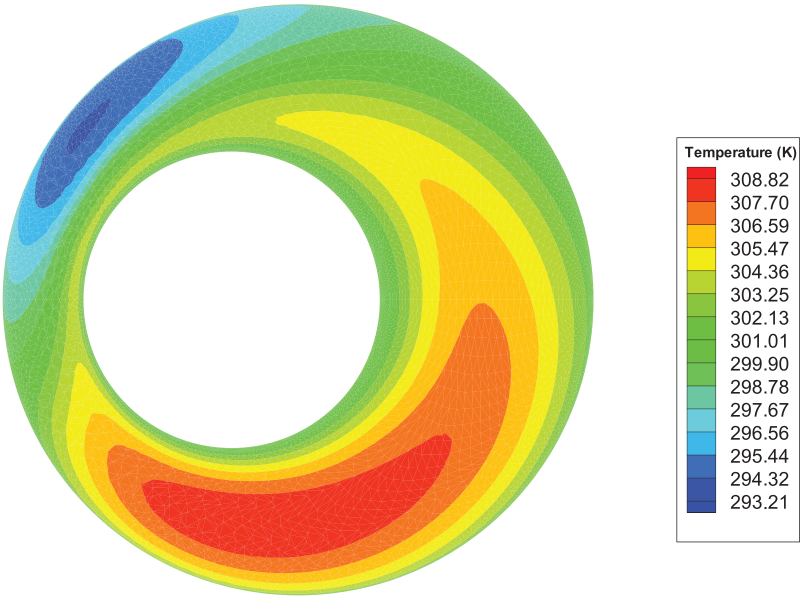

Figure 13. Temperature contour for Mach = 0.5, eccentricity = 0.45, Kn = 0.1

5.6 Stationary body in the rotating flow field

Consider a stationary cylinder of radius *0.01* m placed at a radial location of *0.075* m within a rotating flow confined between outer isothermal rotating cylinders of radius *0.1* m and inner isothermal stationary cylinder of radius *0.05* m. Two cases with subsonic wall speed (Mach = *0.5*) and supersonic wall speed (Mach = *2.0*) with argon gas were chosen for simulation. Figure 14 shows the total *20807* points in the flow domain.

For the case with wall speed of Mach = *0.5* we can observe the spread of the stagnation temperature against the flow and towards the radial direction; it almost covers the whole domain. This happens because the body faces its own wake. Towards the periphery between the rotating cylinder and the stationary cylinder the flow accelerates on the expense of the internal energy, thereby cooling the gas. Figure 15 shows the plot of the temperature contour. Figure 16 shows the Mach contour.

For the case with supersonic wall speed with Mach = *2.0* a vortex ahead of the stationary body in the subsonic pocket can be observed [17,117]. Figure 17 shows the Mach contour and a vortex ahead of the body. At higher speed this vortex becomes weak. It should be noted that the pressure is function of density and entropy per unit mass. If $\nabla\rho \times \nabla p \neq 0$ then, this baroclinic effect creates the vorticity in the subsonic pocket [118]. The baroclinic term χ is derived by taking the curl of the pressure gradient in the Navier-Stokes equation

$$\chi = \nabla \times \left(-\frac{1}{\rho} \nabla p \right) = \frac{1}{\rho^2} \nabla \rho \times \nabla p \cdot \tag{62}$$

Rajput [119] has conducted detailed study to understand the effect of stationary bodies under strong rotation. The size of the sub-sonic pocket becomes small at very high rotational speed. As a consequence a very fine grid is required to capture the weak vortex at very high rotational speed. It should be noted that as the wall speed increases the central core becomes rarefied and non-continuum regions starts appearing.

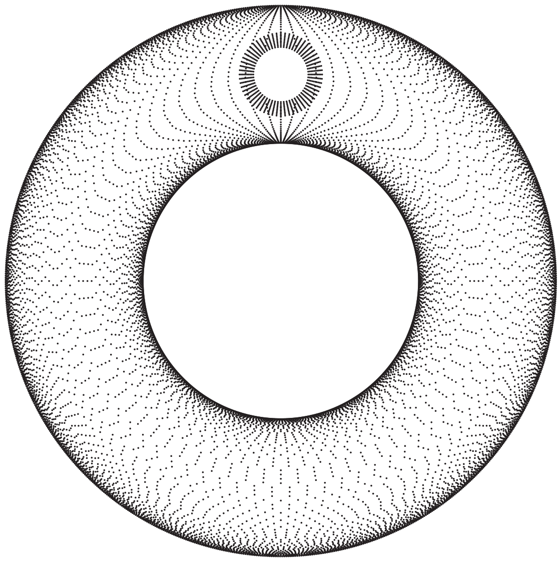

Figure 14. Cloud of points

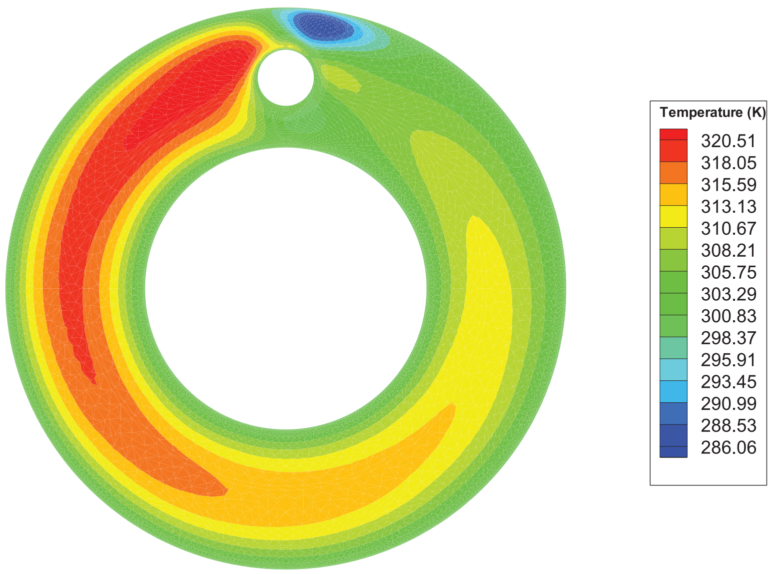

Figure 15. Temperature contour

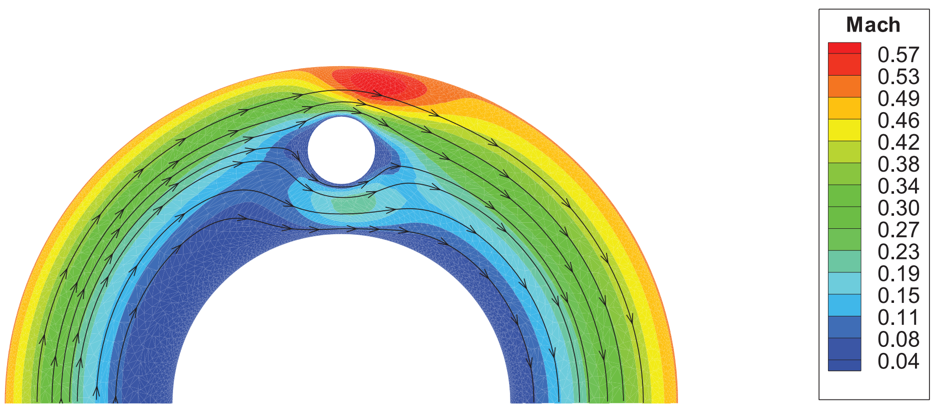

Figure 16. Mach contour for subsonic case

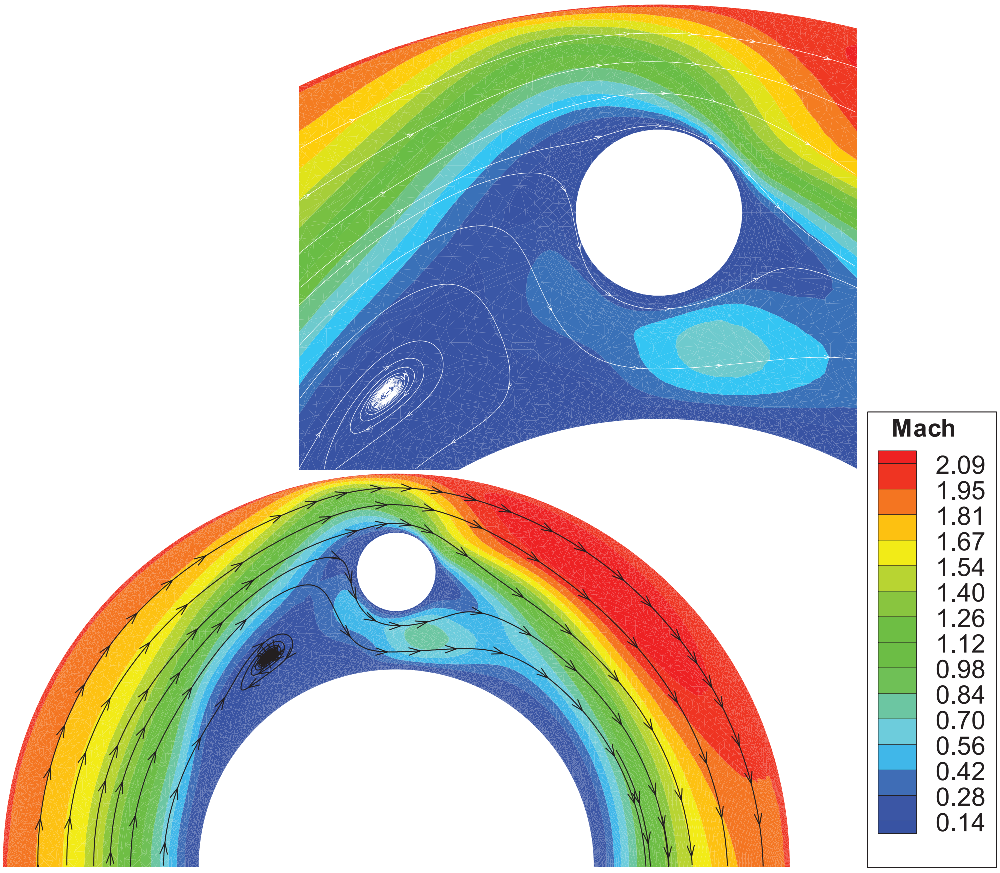

Figure 17. Mach contour for supersonic case with the zoom view near the stationary body showing the vortex

In the three dimensional case due to relieving effect of flow moving out axially the effect of shock is not so severe. For example consider an hemisphere of radius *0.005* m placed mid way at a radius of *0.075* m in a annular cylindrical sector of outer radius *0.1* m and inner radius of *0.05* m and height of *0.035* m rotating at *2000* revolutions per second with density of air at wall being *0.01271* Kg/m^3. Figure 18 shows the points generated using cylindrical and spherical meshes, the total number of points in the cloud was *122921*.

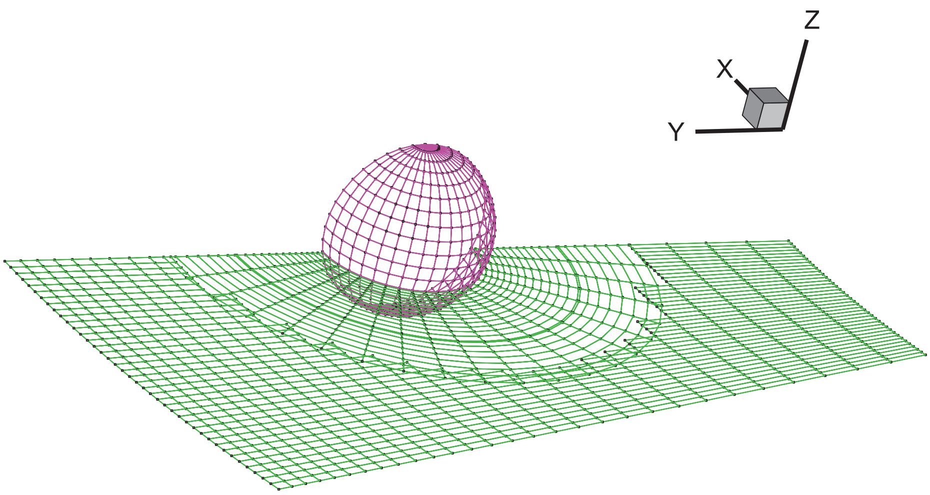

Figure 18. Cloud of points generated using cylindrical and spherical mesh

Figure 19. shows the non-continuum transition region ($Kn > 0.1$) due to the development of rarefied core at high speed. This region requires corrections with Burnett terms to the first order kinetic slip boundary condition. More appropriate way to simulate this region is to couple the Navier-Stokes solver with either DSMC or Boltzmann equation. In the present case far-field boundary condition uses incoming distribution as Maxwellian (approximating the interior rarefied core as collisonless region) and outgoing distribution as Chapman-Enskog as described in Part 1 of the paper. Figure 20 shows the contours of density. Figure 21 shows the Mach contours. The shock is smeared due to coarse distribution of points. Figure 21 also shows that the subsonic pocket which is smaller due to the choice of the flow domain. The effect of shock is not so severe because of the relieving effect of three dimensional geometry. This test case even with a coarse cloud of points demonstrates the robustness of the m-SLKNS solver using VRKFVS scheme in handling the entire stretch of the flow from supersonic region to rarefied non-continuum regions.

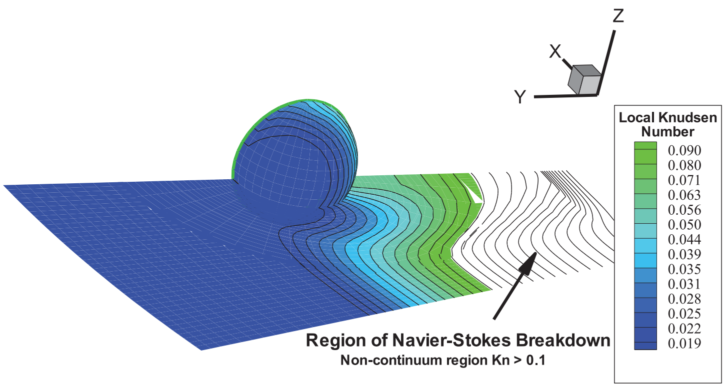

Figure 19. Region of non-continuum transition region

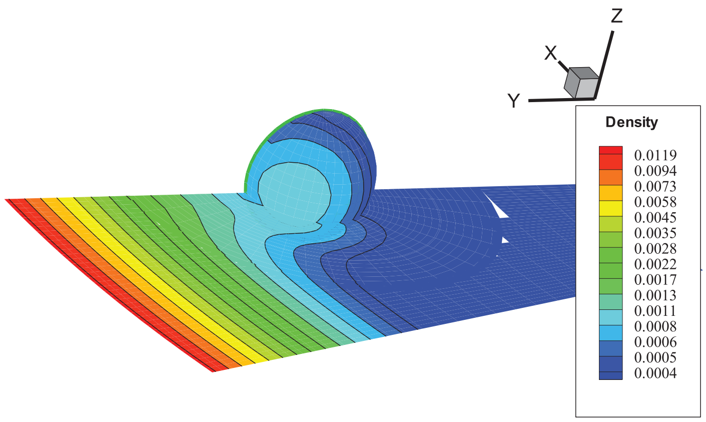

Figure 20. Plot of density

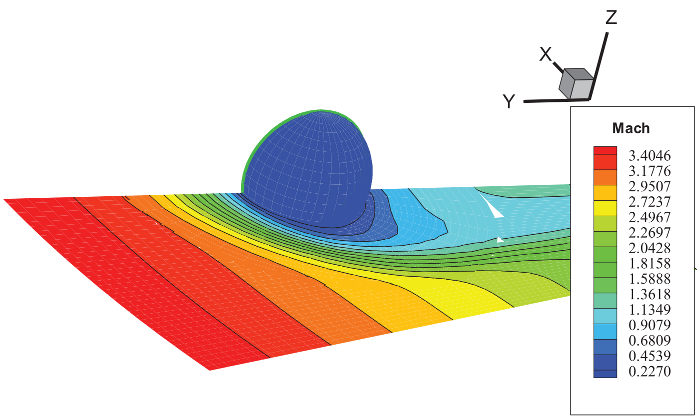

Figure 21. Mach contours

6. CONCLUSIONS

There are many approaches for numerical flow modeling of slip and rarefied flows. Molecular based approach is computationally expensive compared to continuum solver based approach. The slip flow simulation using the continuum solver can be carried out either by using slip models or implementing kinetic wall boundary condition. It can be seen that there are large number of second order slip models existing in the literature each with its own slip coefficients and range of validity in the non-continuum slip and the transition region. Most of these slip models are for simple micro-channel flows without any flow separation. More-so-ever slip boundary condition should effectively capture slip flow features under combined effects of adverse pressure gradient and rarefaction. The Kinetic Flux Vector Splitting (KFVS) scheme with kinetic slip flow boundary condition was found very useful in simulating rotating slip flows. The approach of adding second order Kn^2 terms associated with the Burnett constitutive relations to KFVS based slip boundary condition needs further investigations. Since the real life problems have difficult geometry and grid generation for such geometries becomes a bottleneck, the meshless method based on least square approach was able to handle stretched connectivity and simulate many problems of interest.

The solver also uses Variance Reduction Kinetic Flux Vector Splitting (VRKFVS) scheme to capture slip flow features and typical features of the strongly rotating flows characterized by steep density gradient, supersonic flows and thin boundary layers towards the peripheral region with a rarefied central core. Development of hybrid solver by coupling the rarefied region with the particle solver or by direct numerical solution of Boltzmann equation will be the part of the future scope of the study.

7. ACKNOWLEDGEMENTS

The first author is grateful to Prof. S.M. Deshpande, Prof. J.C. Mandal, Mr. T.K.Bera and Mr. A. Sanyal for encouragement and their support.

REFERENCES

1. Bark F.H., Bark T.H. On vertical boundary layers in a rapidly rotating gas. Journal of Fluid Mechanics 1976, 78, 815-825.
2. Brouwers J.J.H. On compressible flow in a rotating cylinder. Journal of Engineering Mathematics 1978, 12,265-285.
3. Dickinson G.J. , Jones I.P. Numerical solutions for the compressible flow in a rapidly rotating cylinder. Journal of Fluid Mechanics 1981, 107,89-107.
4. Park J.S, Hyun J.M. Flow of a compressibl fluid in a rapidly rotating pipe with azimuthally varying wall thermal condition. Journal of Fluid Mechanics 2004,518,125-145
5. Babarsky R.J, Herbst I.W, Wood III H.G. A new variational approach to gas flow in a rotating system. Physics of Fluid 2002,14(10),3624-3640.
6. Johnson EA, Stopford P.J. Shear flow in the presence of 'strong rotation': II. Approximations for continuum-plus-rarefied flow . J. Phys. D: Appl. Phys. 1983, 16,1207—1215.
7. Müller I., On the frame dependence of stress and heat flux., Arch. Rational Mech. Anal. 45, 1972,241-250
8. Sharipov F.M., Kremer G.M., Non-isothermal Couette flow of a rarefied gas between two rotating cylinders. Eur. J. Mech. B/Fluids 1999, 18(1), 121-130.
9. Sharipov F.M, Cumin L.M.G., Kremer G.M. Transport phenomena in rotating rarefied gases Physics of Fluids 2001,13(1),335-346.
10. Sharipov F.M., Kremer G.M. On thr frame dependence of constitutive equations. I. Heat transfer through a rarefied gas between two rotating cylinders.,Continuum Mechanics. Thermodynamics, 7,1995,57-71.
11. Taheri P, Struchtrup H. Effects of rarefaction in microflows between coaxial cylinders. Physical Review E 2009, 80,066317(1)-066317(16).
12. Ghosh AK, Deshpande SM. Least squares kinetic upwind method for inviscid compressible flows. AIAA paper 95-1735,1995.
13. Ramesh V. Least squares grid-free kinetic upwind method. PhD thesis. Bangalore, Dept. of Aerospace Engg., Indian Institute of Science, 2001.

14. Ramesh V, Deshpande SM,Unsteady flow computations for flow past multiple moving boundaries using LSKUM, Computers and Fluids, 2007,36, 1592–1608.
15. Praveen C, Ghosh AK, Deshpande SM. Positivity preservation, stencil selection and applications of LSKUM to 3-D inviscid flows. Computers and Fluids 2009,38(8),1481-1494.
16. Praveen C. Development and Applications of Kinetic Meshless Methods for Euler Equations. PhD thesis. Bangalore: Dept. Of Aerospace Engg., Indian Institute of Science, 2004.
17. Mahendra AK. Application of least squares kinetic upwind method to strongly rotating viscous flows. M.Sc.(Eng) Thesis. Indian Institute of Science, Bangalore,2003 .
18. Mahendra AK, Singh RK, Gouthaman G. Meshless kinetic upwind method for compressible viscous rotating flows. Comput Fluids, in press. doi:10.1016/j.compfluid.2010.10.015.
19. Anil N., Rajan NKS, Deshpande S.M., Mathematical analysis of dissipation in m-KFVS Method, Fluid Mechanics Report 2005 FM 1, Indian Institute of Science, Bangalore,2005
20. Kolobov VI, Arslanbekov RR, Aristov V, Frolova AA, Zabelok SA. Unified solver for rarefied and continuum flows with adaptive mesh and algorithm refinement. Journal of Computational Physics, 2007,223,589-608.
21. Wang W-L,Boyd I.D, Predicting continuum breakdown in hypersonic viscous flows, Physics of fluids,2003,15(1),91-100.
22. Schwartzentruber, T. , Boyd, I. A hybrid particle-continuum method applied to shock waves. Journal of Computational Physics, 2006, 215,402-416.
23. Lockerby D.A., Struchtrup H, Reese J.M., Switching criteria for hybrid rarefied gas flow solvers, Rarefied Gas Dynamics:26th International Symposium, ed. T. Abe, 2009, CP1084,434-440.
24. Arkilic EB, Schmidt M.A., Breuer KS. Gaseous Slip Flow in Long Microchannels. Journal of Microelectromechanical systems, 1997, 6(2), 167-178.
25. M. Gad-el Hak. The Fluid Mechanics of Microdevices - The Freeman Scholar Lecture. ASME Journal of Fluids Engineering, 1999, 121(403), 5-33.
26. Bird, GA. Molecular Gas Dynamics and the Direct Simulation of Gas Flows,Clarendon, Oxford, 1994.
27. Shen, C. Rarefied Gas Dynamics : Fundamentals, Simulations and Micro Flows. Springer, Berlin,2005.
28. Aristov, V. V. Direct methods for solving the Boltzmann equations and study of non equilibrium flows, Kluwer,2001.
29. Burt JM, Boyd ID, A hybrid particle approach for continuum and rarefied flow simulation, Journal of Computational Physics 2009, 228,460–475.
30. Cercignani C, Lampis M, and Lorenzani S, Variational approach to gas flows in microchannels, Physics of Fluids 2004,16(9), 3426-3437
31. Fan, J., Shen, C. Statistical simulation of low-speed unidirectional flows in transition regime. In: Rarefied Gas Dynamics, edited by R. Brun *et al*., 1999,vol. 2, 245. Cepadus-Editions, Toulouse.
32. Fan, J. , Shen, C. Statistical simulation of low-speed rarefied gas flows. Journal of Computational Physics, 2001, 167, 393.
33. Goldstein DB, Sturtevant B, Broadwell JE, Investigation of the motion of the discrete velocity gases, In: E.P. Muntz *et al*. (Eds.), Proceedings of the16th International Symposium on RGD, in Series: Progress in Astronautics and Aeronautics 118, 1989, 100.
34. Rogier F., Schneider JA, A direct method for solving Boltzmann equation, Trans. Theo. Stat. Phys., 1994, 23 (1–3), 313–338.
35. Tan Z., Varghese PL, The Δ–e method for the Boltzmann equation, J. Comput. Phys.,1994, 110, 327.
36. Tcheremissine F.G., Solution to the Boltzmann kinetic equation for high-speed flows, Comput. Math. Math. Phys. 2006,4, 315.
37. Degond P., Pareschi L., Russo G.(Eds.), Modeling and Computational methods for Kinetic Equations, Birkhauser, Boston, 2004, 356.
38. Oran, E. S., Oh, C. K. , Cybyk, B. Z. Direct simulation Monte Carlo: recent advances and applications. Annu. Rev. Fluid Mech. 1998, 30, 403–441.

39. Crouseilles N., Degond P., Lemou M., A hybrid kinetic/fluid models for solving the gas dynamics Boltzmann–BGK equation, J. Comput. Phys. 2004, 199,776.
40. Beylich AE, Solving the kinetic equation for all Knudsen numbers, Physics of Fluids,2000, 12(2) ,444-465
41. Hash DB, Hassan HA, Two-dimensional coupling issues of hybrid DSMC/Navier–Stokes solvers, AIAA paper 97-2507, 1997.
42. Lockerby, D., Reese, J. , Gallis, M. The usefulness of higher order constitutive relations for describing the Knudsen layer. Physics of Fluids, 2005,17, 100609(1)–100609(9).
43. Chapman, S. , Cowling, T.G. The Mathematical Theory of Non-Uniform Gases. Cambridge University Press, Cambridge,1970.
44. Wang Chang, C.S. On the theory of the thickness of weak shock waves, Technical report no. APL/JHU, CM-503. Dept. of Eng. Research, University of Michigan, 1948.
45. Grad, H. On the Kinetic theory of rarefied gases. Commun. Pure Appl. Maths 1949,2,331.
46. Wood L.C. Frame-indifferent kinetic theory. Journal of Fluid Mechanics,1983,136, 423–433.
47. Lumpkin III, F. Development and evaluation of continuum models for translational-rotational nonequilibrium. Ph.D. thesis, Stanford University, 1990
48. Eu, C. Kinetic Theory and Irreversible Thermodynamics. Wiley, New York,1992.
49. Cercignani, C. Mathematical Methods in Kinetic Theory. Plenum, New York.,1990
50. Cercignani, C. Higher order slip according to the linearized Boltzmann equation,Institute of Engineering Research Report AS-64-19, University of California, Berkeley, 1964.
51. Loyalka, S., Petrellis, N. , Storvick, T. Some numerical results for the BGK model: Thermal creep and viscous slip problems with arbitrary accommodation at the surface. Physics of Fluids, 1975,18, 1094–1099
52. Zhong, X., MacCormack, R.W. , Chapman, D.R. Stabilization of the Burnett equations and application to hypersonic flows. AIAA Journal, 1993, 31.
53. Jin, S. , Slemrod, M. Regularization of the burnett equations via relaxation. Journal of Statistical Physics,2001, 103 (5/6), 1009–1033.
54. Struchtrup, H., Torrilhon, M. Regularization of Grad's 13 moment equations: derivation and linear analysis. Physics of Fluid, 2003,15. 33
55. Balakrishnan R. An approach to entropy consistency in second-order hydrodynamic equations. Journal of Fluid Mechanics 2004, 503,201-245.
56. Hadjiconstantinou N.G., The limits of Navier-Stokes theory and kinetic extensions for describing small-scale gaseous hydrodynamics, Physics of Fluids,2006,18,111301(1)-111301(19).
57. Loyalka S.K., Velocity profile in the Knudsen layer for the Kramer's problem, The Physics of Fluids, 1975,18(12),1666-1669.
58. Harley J.C, Huang Y, Bau H, and Zemel J.N., Gas flow in microchannels, J. Fluid Mech., 1995, 284, 257–274
59. Arkilic E.B., Breuer K.S., Schmidt M.A., Gaseous Flow in Microchannels,1994, ASME FED-Vol. 197, Application of Microfabrication to Fluid Mechanics, pp. 57- 66
60. Beskok A. and Karniadakis G., Simulation of heat and momentum transfer in micro-geometries, 1993, AIAA Paper 93-3269.
61. Maxwell, J. On stresses in rarefied gases arising from inequalities of temperature. Philosophical Transactions Royal Society of London, 1879,170, 231–256.
62. Lockerby DA, Reese JM, Emerson DR, Barber RW. Velocity boundary condition at solid walls in rarefied gas calculations. Physical Review E 2004, 70,017303(1)-017303(4).
63. Kennard E.H., Kinetic Theory of Gases, McGraw-Hill, New York, 1938.
64. Albertoni S., Cercignani C., Gotusso L., Numerical Evaluation of the slip coefficient, Physics of Fluids,1963, 6, 993–996.
65. Loyalka S.K., Hickey K.A., Plane Poiseuille flow: Near continuum results for a rigid sphere gas, Physica A 1989, 160, 395.

66. Loyalka S.K., Tompson R.V., The velocity slip problem: Accurate solutions of the BGK model integral equation, European Journal of Mechanics B/Fluids, 2009, 28 , 211–213
67. Ohwada T, Sone Y., Aoki K., Numerical analysis of the Poiseuille and thermal transpiration flows between two parallel plates on the basis of the Boltzmann equation for hard-sphere molecules,Physics of Fluids A,1,1989,2042-2049.
68. Hadjiconstantinou N.G., Comment on Cercignani's second-order slip coefficient, Physics of Fluids 2003,15(8),2352-2354.
69. Deissler R.G., An analysis of second-order slip flow and temperature jump boundary conditions for rarefied gases, Int. J. Heat Mass Transfer, 1964,7,681–694.
70. Maurer J., Tabeling P., Joseph P., Willaime H., Second-order slip laws in microchannels for helium and nitrogen, Physics of Fluids,2003, 15(9), 2613-2621.
71. Ewart T, Perrier P, Graur I.A., Meolans J.G., Mass flow rate measurements in a microchannel, from hydrodynamic to near free molecular regimes,J. Fluid Mech. 584,2007,337.
72. Beskok A, Validation of a new velocity-slip model for separated gas microflows, Numerical heat transfer, Part B, 2001,40,451-471.
73. Agrawal A, Djenidi L, Antonia R.A., Simulation of gas flow in microchannels with a sudden expansion or contraction, J. Fluid Mech.,2005, 530, 135–144.
74. Struchtrup, H., Torrilhon, M. Higher-order effects in rarefied channel flows,Physical Review E, 2008, 78, 046301(1)-046301(11).
75. Cercignani C., and Lorenzani S., Variational derivation of second-order slip coefficients on the basis of the Boltzmann equation for hard-sphere molecules, Physics of Fluids,2010, 22,062004(1)-062004(8)
76. Schamberg R, The Fundamental Differential Equations and the Boundary Conditions for High Speed Slip-Flow, and Their Application to Several Specific Problems, Ph.D. thesis, California Institute of Technology, Pasadena, CA, 1947.
77. Sreekanth A.K., Slip flow through long circular tubes, in: L. Trilling, H.Y. Wachman (Eds.), Proceedings of the sixth international symposium on Rarefied Gas Dynamics, Academic Press, 1969, 667–680.
78. Lang, H., Second order slip effects in Poiseuille flow, Physics of Fluids, 1976,19,366-371
79. Aubert C., Colin S., High-order boundary conditions for gaseous flows in rectangular microducts, Microscale Thermophys. Eng. 5,2001,41-54.
80. Hsia Y.T., Domoto G.A., An Experimental Investigation of Molecular Rarefaction Effects in Gas Lubricated Bearings at Ultra Low Clearances, J. Lubrication Technol., 1983,105,120-130.
81. Mitsuya Y, Modified Reynolds equation for ultra-thin film gas lubrication using 1.5-order slip-flow model and considering surface accommodation coefficient, Journal of Tribology,1983, 115,289–294.
82. Pan L.S., Liu G.R., Lam K.Y., Determination of slip coefficient for rarefied gas flows using direct simulation Monte Carlo, J .Micromech. Microeng. ,1999, 9, 89–96.
83. Hadjiconstantinou N.G., Al-Mohssen H.A., A linearized kinetic formulation including a second-order slip model for an impulsive start problem at arbitrary Knudsen numbers, J. Fluid Mechanics ,2005, 533, 47-56.
84. Dongari N., Agrawal A., Agrawal A., Analytical solution of gaseous slip flow in long microchannels International Journal of Heat and Mass Transfer, 2007, 50, 3411–3421.
85. Karniadakis G.E., Beskok A., Aluru N., Microflows and Nanoflows: Fundamentals and Simulation, Springer-Verlag, New York, 2005.
86. Roohi E., Darbandi M., Extending the Navier–Stokes solutions to transition regime in two-dimensional micro- and nanochannel flows using information preservation scheme, Physics of Fluids,2009, 21, 082001(1)-082001(12).
87. Fichman M, Hetsroni G., Viscosity and slip velocity in gas flow in microchannels, Physics of Fluids, 2005, 17, 123102(1)-123102(5).
88. Lilley C.R., Sader J.E., Velocity profile in the Knudsen layer according to the Boltzmann equation, Proc. of the Royal Society A, 2008, 464,2015-2035.

89. Meng J, Zhang Y, Analytical Solution for the Lattice Boltzmann Model Beyond Naviers-Stokes, Advances in Applied Mathematics and Mechanics, 2010, Vol. 2, No. 5, pp. 670-676.
90. Ansumali S., Karlin I, Kinetic boundary conditions in the lattice Boltzmann method, Physical Review E , 2002, 66, 026311(1)-026311(6).
91. Sbragaglia M, Succi S., Analytical calculation of slip flow in lattice Boltzmann models with kinetic boundary conditions, Physics of Fluids, 2005,17,093602(1)-093602(8).
92. Kim S.H. , Pitsch H., Boyd I.D., Slip velocity and Knudsen layer in the lattice Boltzmann method for microscale flows, Physical Review E,2008,77, 026704 (1)-026704(12).
93. Guo Z, Zheng C, and Shi B, Lattice Boltzmann equation with multiple effective relaxation times for gaseous microscale flow, Physical Review E,2008,77, 036707 (1)-036707(12).
94. Agarwal, R. K., Yun, K.-Y., Balakrishnan, R. Beyond Navier–Stokes: Burnett equations for flows in the continuum–transition regime., Physics of Fluids,2001, 13, 3061–3085.
95. Bao F-B, Lin J-Z, Burnett simulations of gas flow in microchannels, Fluid Dynamics Research,2008, 40, 679–694.
96. Mieussens L. Discrete-Velocity Models and Numerical Schemes for the Boltzmann-BGK Equation in Plane and Axisymmetric Geometries. Journal of Computational Physics 2000, 162,429-466.
97. Lockerby D.A., Reese J.M., High-resolution Burnett simulations of micro Couette flow and heat transfer, Journal of Computational Physics, 2003, 188, 333–347.
98. Xu K, Li Z. Microchannel flow in the slip regime: gas-kinetic BGK-Burnett solutions. Journal of Fluid Mechanics 2004, 513,87-110.
99. Li Z, Zhang H, Gas kinetic algorithm using Boltzmann model equation, Computers & Fluids, 2004, 33, 967–991.
100. Mahendra A.K., Gouthaman G, Singh R.K., Meshless method for slip flows, Report HBNI-3-2010,2010.
101. Arora K. Weighted least squares kinetic upwind method using eigendirections (WLSKUM-ED). Ph.D. Thesis. Indian Institute of Science,2006.
102. Fortunato B, Magi V. An implicit Lambda Method for 2-D Viscous Compressible Flows. In: Fourteenth International Conference on Numerical Methods in Fluid Dynamics, Lecture Notes in Physics , S. M. Deshpande, S. S. Desai, R. Narasimha (eds.), Springer, 1995, 259-264.
103. Catalano LA, De Palma P, Naplitano M, Pascazio G. Genuinely multidimensional upwind methods for accurate and efficient solutions of compressible flows. Notes on Numerical Fluid Mechanism Vieweg-Verlag, Braunschweig, 1997, 221-250.
104. Avci M, Aydin O, Laminar forced convection slip-flow in a micro-annulus between two concentric cylinders, International Journal of Heat and Mass Transfer, 2008, 51, 3460-3467.
105. Einzel D, Panzer P, Liu M, Boundary Condition for fluid flow : Curved or Rough surfaces, Phys. Rev. Lett., 1990, 64, 2269-2272.
106. Tibbs KW, Baras F, Garcia AL. Anomalous flow profile due to the curvature effect on slip length. Physical Review E, 1997, 56(2), 2282-2283.
107. Aoki K, Yoshida H, Nakanishi T, Garcia A.L. , Inverted velocity profile in the cylindrical Couette flow of a rarefied gas, Physical Review E , 2003, 68, 016302(1)-016302(11).
108. Wannier GH. A contribution to the hydrodynamics of lubrication. Quarterly Journal of Applied Mathematics, 1950,8, 1-32.
109. Kamal MM. Separation in the flow between eccentric rotating cylinders. Journal of Basic Engineering, ASME, 1966,88, 717–724.
110. Wood WW. The asymptotic expansions at large Reynolds numbers for steady motion between non-coaxial rotating cylinders. Journal of Fluid Mechanics, 1957, 8, 159–175.
111. Ballal BY, Rivlin RS. Flow of a Newtonian fluid between eccentric rotating cylinders: inertial effects. Archive of Rational Mechanics and Analysis, 1977, 62, 237–294.
112. Araujo JHC, Ruas V, Vargas AS. Finite element solution of flow between eccentric cylinders with viscous dissipation. International Journal of Numerical Methods in Fluids, 1990,11, 849–865.

113. Ramesh PS, Lean MH. A boundary integral equation method for Navier–Stokes equations. Application to flow in annulus of eccentric cylinders. International Journal of Numerical Methods in Fluids, 1991, 13, 355–369.
114. San Anders A, Szeri AZ. Flow between eccentric rotating cylinders. Journal of Applied Mechanics, ASME, 1984, 51, 869–878.
115. de Socio L.M., Marino L., Numerical experiments on the gas flow between eccentric rotating cylinders, International Journal for Numerical Methods in Fluids, 2000, 34,229–240.
116. de Socio L.M., Marino L., Flow separation between rotating eccentric cylinders, European Journal of Mechanics B/Fluids,2003, 22, 85–97.
117. Deshpande S.M, Current Status and Future Directions in CFD, INS Golden Jubilee Lecture, Mumbai, 2004.
118. Mahendra AK, Sanyal A, Gouthaman G. , Parallel meshless solver for strongly rotating flows. In: Proceedings The 9th International workshop on Separation phenomena in liquids and gases, S. Zeng (ed.), Tsinghua University Press, Beijing, 2006,127-131.
119. Rajput S.,Study of shocks under strong rotation, M.Tech. Thesis, Homi Bhabha National Institute, Mumbai, 2010.